doi:10.1038/nature16072

Liquids with permanent porosity

This file includes:

1. General synthetic & analytical methods
2. Synthesis and characterization of the crown ether cage
3. Molecular simulations for the crown-cage porous liquid
4. Positron annihilation lifetime spectroscopy (PALS) experiments
5. Measurement of gas solubilities in the crown-cage porous liquid
6. Scrambled cages: synthesis, characterization, gas solubilities, and guest selectivities

Supplementary Figures 1–36

Supplementary Tables 1–14

1. General synthetic & analytical methods

Materials: 1,3,5-Triformylbenzene was purchased from Manchester Organics (UK) and used as received. Other chemicals were purchased from TCI UK or Sigma-Aldrich and used as received. Solvents were reagent or HPLC grade purchased from Fisher Scientific, with the exception of anhydrous solvents, which were purchased as sure-seal bottles from Sigma-Aldrich. These were used as received unless specificed.

Synthesis: All reactions requiring anhydrous or inert conditions were performed in oven-dried apparatus under an inert atmosphere of dry nitrogen, using anhydrous solvents introduced into the flask using disposable needles and syringes. All reactions were stirred magnetically using Teflon-coated stirring bars. Where heating was required, the reactions were warmed using a stirrer hotplate with heating blocks with the stated temperature being measured externally to the reaction flask with an attached probe. Removal of solvents was done using a rotary evaporator.

TLC and column chromatography: Reactions were monitored by thin layer chromatography (TLC), conducted on pre-coated aluminium-backed plates (Merck Kieselgel 60 with fluorescent indicator UV254). Spots were visualized either by quenching of UV fluorescence or by staining with potassium permanganate. Flash column chromatography was performed manually with silica gel 60 (40-63 μm particle size) applying head pressure by means of nitrogen, or on a Biotage Isolera with KP-Sil Normal Phase disposable columns.

Melting points: Obtained using Griffin melting point apparatus and are uncorrected.

IR spectra: Infra-red (IR) spectra were recorded on a Bruker Tensor 27 FT-IR using ATR measurements for oils and solids as neat samples.

NMR spectra: ^{1}H Nuclear magnetic resonance (NMR) spectra were recorded using an internal deuterium lock for the residual protons in $CDCl_3$ (δ = 7.26 ppm) at ambient probe temperature using either a Bruker Avance 400 (400 MHz) or Bruker DRX500 (500 MHz) instrument.

NMR data are presented as follows: chemical shift, integration, peak multiplicity (s = singlet, d = doublet, t = triplet, q = quartet, m = multiplet, br = broad, app = apparent), coupling constants (*J* / Hz) and assignment. Chemical shifts are expressed in ppm on a δ scale relative to δ_{CDCl3} (7.26 ppm) and coupling constants, *J*, are given in Hz. Assignments were determined either on the basis of unambiguous chemical shift or coupling patterns or by analogy to fully interpreted spectra for structurally related compounds.

^{13}C NMR spectra were recorded using an internal deuterium lock using $CDCl_3$ (δ = 77.16 ppm) at ambient probe temperatures using either a Bruker Avance 400 (101 MHz) or Bruker DRX500 (126 MHz) instrument.

MS / HRMS: Electrospray ionization mass spectrometry (ES-MS) was carried out using either a Waters Micromass Electrospray LCT mass spectrometer (MeOH, 40 V cone voltage) or an Agilent Technologies 6530B accurate-mass QTOF Dual ESI mass spectrometer (MeOH + 0.1% formic acid, capillary voltage 5000-4000 V, fragmentor 225-150 V) both in positive-ion detection mode.

Elemental analysis: Performed using a Thermo Flash EA1112 (FEA) (University of Liverpool analytical services).

HPLC: High-performance liquid chromatography (HPLC) was conducted on a Dionex UltiMate 3000 equipped with a diode array UV detector using a Thermo-Scientific Syncronis C8 column, 150x4.6 mm, 3 μm (SN 10136940, Lot 12459). The mobile phase was isocratic MeOH at a flow rate of 1 $mL.min^{-1}$ for a 10 min run time. The injection volume was 5 μL and the sample concentration was 1 $mg.mL^{-1}$. Detection for UV analysis was conducted at 254 nm.

TGA: Thermogravimetric analysis (TGA) was carried out using a Q5000 IR analyser (TA instruments) with an automated vertical overhead thermobalance. The samples were heated at the rate of 5 °C/min to 550 °C in an aluminium pan under a nitrogen flow. All solid materials were desolvated by heating to 90 °C in a vacuum oven overnight prior to TGA analysis.

DSC: Differential scanning calorimetry (DSC) was carried out using a Q2000 analyser (TA instruments). The samples were heated at the rate of 5 °C/min to 300 °C in Tzero sealed-aluminium pans under a nitrogen flow (50 mL/min). Measurements were repeated a minimum of three times with the onset temperature of thermal decomposition and the associated energy release reported.

Viscosity: Viscosity measurements were carried out using a calibrated RheoSense μVISC viscometer (0.01–100 cP) with a temperature controller (18–50 °C). Measurements were repeated a minimum of three times. The average viscosity is reported with the standard deviation displayed as error bars in **Supplementary Figures 2.9 & 2.10**.

2. Synthesis and characterization of the crown ether cage

2.1. Synthesis of the crown ether diamine

The crown-ether diamine, **S5**, was prepared according to the following scheme:

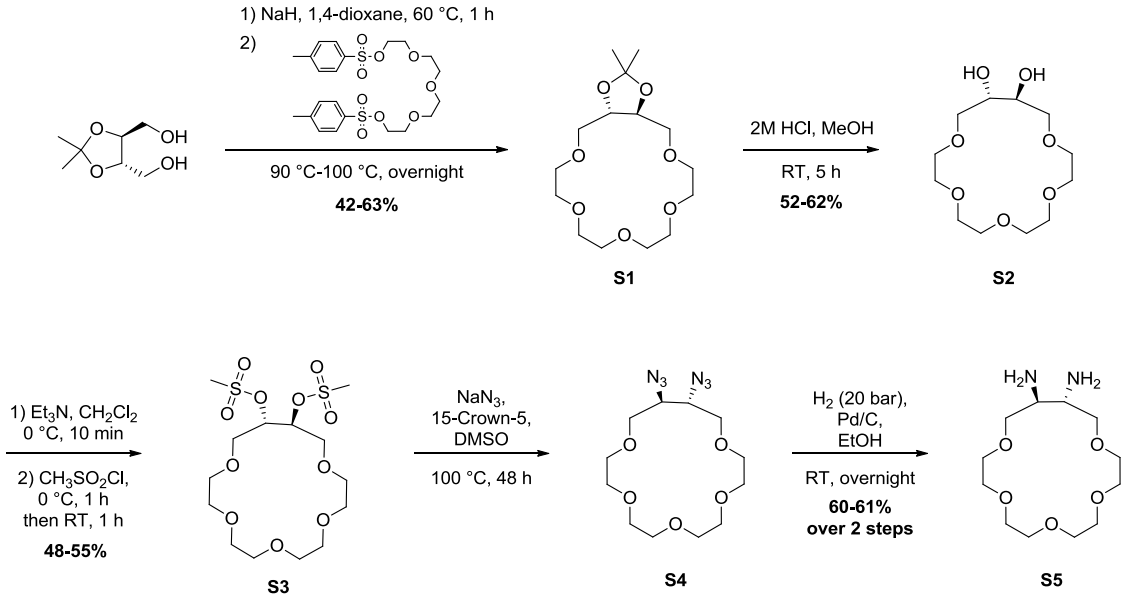

The individual reaction steps in this scheme are described in detail below.

(3a*S*,18a*S*)-2,2-Dimethyldodecahydro-[1,3]dioxolo[4,5-*o*][1,4,7,10,13]pentaoxa-cyclohepta-decine, S1

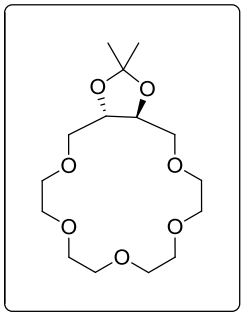

A modification of the procedure of Bogatsky *et al.*[1] was used for this reaction. To a 2 L multineck round bottom flask, equipped with stirrer bar, condenser, was added sodium hydride (4.00 g, 60% dispersion in mineral oil, 100 mmol, 10.0 eq.) under N_2, followed by anhydrous 1,4-dioxane (0.5 L). The suspension was stirred and a solution of (+)-2,3-O-isopropylidene-L-threitol (1.62 g, 10 mmol, 1.0 eq.) in anhydrous 1,4-dioxane (10 mL) was added dropwise. The mixture was heated at 60 °C for 1 h before the temperature was further increased to 95 °C and a solution of tetraethylene glycol bis(p-toluenesulfonate) (5.03 g, 10 mmol, 1.0 eq.) in anhydrous 1,4-dioxane (0.25 L) was added dropwise overnight (either by dropping funnel or *via* the use of a peristaltic pump). Overall, the reaction was heated at 95 °C for a total of 22 h before the reaction was allowed to cool to RT, and then further cooled in an ice-bath before water was added dropwise to quench the residual sodium hydride. The reaction was concentrated *in vacuo* and the residue partitioned between $CHCl_3$ (200 mL) and water (100 mL). The organic phase was separated, and the aqueous layer extracted with $CHCl_3$ (3 × 100 mL) before the combined organic phases were dried (Na_2SO_4) and concentrated *in vacuo*. Purification via column chromatography (DCM/MeOH (95:5)) afforded the desired product, **S1**, as a pale yellow oil (1.848 g, 5.76 mmol, 57 %). Note that this reaction was repeated multiple times on this scale with the typical yield being in the range 42–63 %.

R_f 0.43 (DCM/MeOH; 95:5); **IR** (ν_{max}/cm^{-1}) 2868, 1456, 1373, 1246, 1119, 1079, 986, 927, 849; **^{1}H NMR** (500 MHz, $CDCl_3$) δ_H 4.00–3.95 (2H, m), 3.81–3.78 (2H, m), 3.75–3.71 (2H, m), 3.69–3.60 (16H, m), 1.40 (6H, s); **^{13}C NMR** (101 MHz, $CDCl_3$) δ_C 109.67, 77.63, 72.48, 71.33, 70.91, 70.83, 70.74, 27.09; **HRMS** (ES+) calc. for $C_{15}H_{28}NaO_7$ $[M+Na]^+$ 343.1733, found 343.1730; **CHN Analysis** calc. for $C_{15}H_{28}O_7$: C, 56.23; H, 8.81; found: C, 55.86; H, 8.80.

(15*S*,16*S*)-1,4,7,10,13-Pentaoxacycloheptadecane-15,16-diol, S2

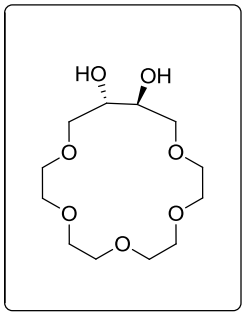

Again, a modification of the procedure of Bogatsky *et al.*[1] was used for this reaction. To a stirred solution of the acetal, **S1** (4.05 g, 12.64 mmol, 1.0 eq.) in MeOH (17 mL) was added an *aq.* 2 M HCl solution (5.3 mL). The colourless solution was allowed to stir at RT overnight (18 h) before the methanol and the acetone that is produced were removed under reduced pressure. The resulting residue was partitioned between $CHCl_3$ (100 mL) and sat. *aq*. $NaHCO_3$ solution (40 mL) and the organic phase separated. The aqueous layer was further extracted with $CHCl_3$ (3 × 100 mL) before the combined organic phases were dried ($MgSO_4$) and concentrated *in vacuo* to afford the diol, **S2**, as a pale yellow oil (2.21 g, 7.88 mmol, 62 %). Note that the diol product appeared to be partially water soluble. The reaction was repeated multiple times on this scale with the typical yield being 52–62 %.

R_f 0.23 (DCM/MeOH; 95:5); **IR** (ν_{max}/cm^{-1}) 3430 (br), 2865, 1452, 1351, 1296, 1249, 1097, 987, 941, 879; **^{1}H NMR** (500 MHz, $CDCl_3$) δ_H 3.87–3.80 (2H, m), 3.77–3.71 (2H, m), 3.71–3.57 (18H, m), 3.15 (2H, d, J = 4.8 Hz); **^{13}C NMR** (126 MHz, $CDCl_3$) δ_C 72.45, 70.82, 70.75, 70.63, 70.62, 70.53; **HRMS** (ES+) calc. for $C_{12}H_{24}NaO_7$ $[M+Na]^+$ 303.1420, found 303.1418; **CHN Analysis** calc. for $C_{12}H_{24}O_7$: C, 51.42; H, 8.63; found: C, 51.25; H, 8.85.

(15*S*,16*S*)-1,4,7,10,13-Pentaoxacycloheptadecane-15,16-diyl dimethanesulfonate, S3

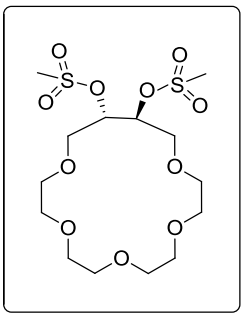

To an ice-cooled solution of diol **S2** (2.21 g, 7.88 mmol, 1.0 eq.) in anhydrous DCM (46 mL) under a N_2 atmosphere was added triethylamine (5.5 mL, 39.42 mmol, 5.0 eq.) dropwise. The resulting solution was stirred for 10 mins at 0 °C before the dropwise addition of methanesulfonyl chloride (3.05 mL, 39.42 mmol, 5.0 eq.). After complete addition, the reaction mixture was stirred at 0 °C for 1 h, and then an RT for 1 h, before being quenched with an *aq*. 1M HCl solution (50 mL). The organic layer was separated and the aqueous layer extracted with DCM (2 × 100 mL) before the combined organic phases were washed with sat. *aq*. $NaHCO_3$ (50 mL), dried ($MgSO_4$), and then concentrated *in vacuo*. Purification via column chromatography (DCM/MeOH; 98:2) afforded the desired product, **S3**, as a pale yellow solid (1.89 g, 4.34 mmol, 55 %). This reaction was repeated multiple times with the typical yield being 48–55 %.

R_f 0.16 (DCM/MeOH; 98:2); **mpt** 57-63 °C; **IR** (ν_{max}/cm^{-1}) 2874, 1468, 1340, 1251, 1173, 1110, 1029, 970, 912; **^{1}H NMR** (500 MHz, $CDCl_3$) δ_H 5.03–4.98 (2H, m), 3.94 (2H, ddd, *J* = 11.6, 3.5, 1.6 Hz), 3.87 (2H, ddd, *J* = 11.6, 2.5, 1.1 Hz), 3.77 (1H, dd, *J* = 5.0, 2.7 Hz), 3.75 (1H, t, *J* = 3.7 Hz), 3.70–3.61 (14H, m), 3.12 (6H, s); **^{13}C NMR** (126 MHz, $CDCl_3$) δ_C 79.19, 71.23, 71.07, 70.94, 70.78, 69.99, 38.85; **HRMS** (ES+) calc. for $C_{14}H_{28}NaO_{11}S_2$ $[M+Na]^+$ 459.0971, found 459.0964; **CHN Analysis** calc. for $C_{14}H_{28}O_{11}S_2$: C, 38.52; H, 6.47; S, 14.69; found: C, 38.71; H, 6.46; S, 14.56.

(15*S*,16*S*)-15,16-Diazido-1,4,7,10,13-pentaoxacycloheptadecane, S4

***Safety note*: Azides can be explosive and appropriate primary and secondary containment should be used that is commensurate with the reaction scale. For example, this reaction was carried out using a blast screen, and the scale per batch was not increased beyond that stated below. Scale up of such reactions should be approached with due caution. It is also important not to approach the onset decomposition temperature (see below).**

DSC Analysis: This was carried out for both the dimesylate starting material, **S3**, and diazide product **S4** (synthesised initially on a small scale) to determine the onset temperature of thermal decomposition and the associated energy release.

	Onset of thermal decomposition	Heat of decomposition
Dimesylate starting material, **S3**	~200 °C	1002–1250 J/g
Diazide product, **S4**	~175 °C	961–1178 J/g

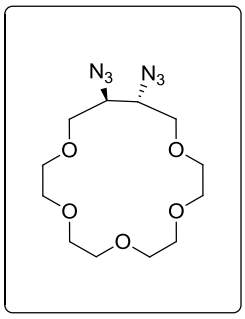

To a wide-neck round bottom flask, equipped with stirrer bar was added sodium azide (1.35 g, 20.87 mmol, 4.8 eq.) under a N_2 atmosphere, followed by anhydrous DMSO (2.6 mL). In a separate flask, the dimesylate **S3** (1.89 g, 4.34 mmol, 1.0 eq.) was dissolved in anhydrous DMSO (7.5 mL) before the addition of 15-crown-5 (85 μL, 0.434 mmol, 0.1 eq.). The dimesylate solution was then added to the azide solution and the reaction mixture heated to 100 °C for 48 h behind a blast screen, before cooling to RT. Analysis of a crude aliquot (quenched in water, extracted with $CDCl_3$ and dried over K_2CO_3) by ^1H NMR spectroscopy was used to confirm full conversion to the diazide product. The reaction was quenched with water (50 mL) and the aqueous layer extracted with Et_2O (3 x 200 mL), before the combined organic layers were washed with water (2 × 200 mL) and dried (Na_2SO_4). The solution was carefully

concentrated to approximately 50 mL under reduced pressure and a small aliquot taken and dried under a N_2 stream for characterisation. The remaining solution had EtOH (100 mL) added and was further concentrated to approximately 20 mL before being used directly without further purification or isolation. For calculation purposes, the yield was assumed to be quantitative for the next hydrogenation step (1.436 g, 4.34 mmol).

R_f 0.23 (DCM/MeOH (98:2)); **IR** (ν_{max}/cm^{-1}) 2870, 2089, 1471, 1356, 1259, 1108, 938; **^{1}H NMR** (500 MHz, $CDCl_3$) δ_H 3.83–3.74 (6H, m), 3.72–3.69 (4H, m), 3.68–3.61 (12H, m); **^{13}C NMR** (126 MHz, $CDCl_3$) δ_C 71.31, 70.99, 70.95, 70.85, 70.74, 61.46; **HRMS** (ES+) calc. for $C_{12}H_{22}N_6NaO_5$ $[M+Na]^+$ 353.1549, found 353.1566.

(15*S*,16*S*)-1,4,7,10,13-Pentaoxacycloheptadecane-15,16-diamine, S5

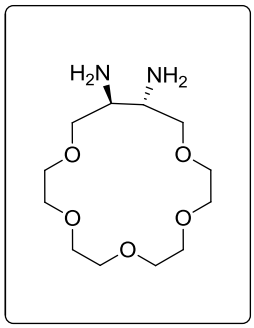

To a vial equipped with stirrer bar was added palladium on carbon (231 mg, 0.217 mmol, 0.05 eq., 10 wt % loading, dry support) under a N_2 atmosphere. To this was added the ethanolic solution of azide **S4** (1.436 g, 4.34 mmol, 1.0 eq.) made up to a total volume of 28 mL using additional EtOH. The uncapped vial was loaded into an autoclave under N_2 and sealed, before the atmosphere was exchanged for hydrogen (20 bar) and the resulting mixture stirred at RT overnight. On completion, the hydrogen atmosphere was exchanged for N_2 before the vial was removed from the autoclave. The catalyst was removed by filtration under N_2 through Whatman glass microfiber filter paper and washed with EtOH (80 mL). Care was taken to avoid the catalyst going dry in air: after the filtration was complete, water was added to the catalyst prior to disposal. The filtrate was concentrated *in vacuo* to afford diamine **S5** as a pale yellow oil (743 mg, 2.67 mmol, 61 % over 2 steps). This reaction was repeated multiple times with the typical yield being 60–61% over 2 steps.

R_f 0.09 (DCM/MeOH (95:5)); **IR** (ν_{max}/cm^{-1}) 3397 (br), 2870, 1587, 1459, 1356, 1296, 1248, 1108, 938; **^{1}H NMR** (400 MHz, $CDCl_3$) δ_H 3.66–3.59 (18H, m), 3.47–3.41 (2H, m), 2.94–2.88 (2H, m, C*H*), 1.70 (4H, br s, N*H*); **^{13}C NMR** (101 MHz, $CDCl_3$) δ_C 74.16, 70.99, 70.86, 70.80, 70.50, 53.22; **HRMS** (ES+) calc. for $C_{12}H_{27}N_2O_5$ $[M+H]^+$ 279.1920, found 279.1933; **CHN Analysis** calc. for $C_{12}H_{26}N_2O_5$: C, 51.78; H, 9.42; N, 10.06; found: C, 50.86; H, 9.41; N, 9.74.

2.2. NMR spectra of crown ether diamine and its intermediates, S1–S5

(3a*S*,18a*S*)-2,2-Dimethyldodecahydro-[1,3]dioxolo[4,5-*o*][1,4,7,10,13]pentaoxa-cyclohepta-decine, S1

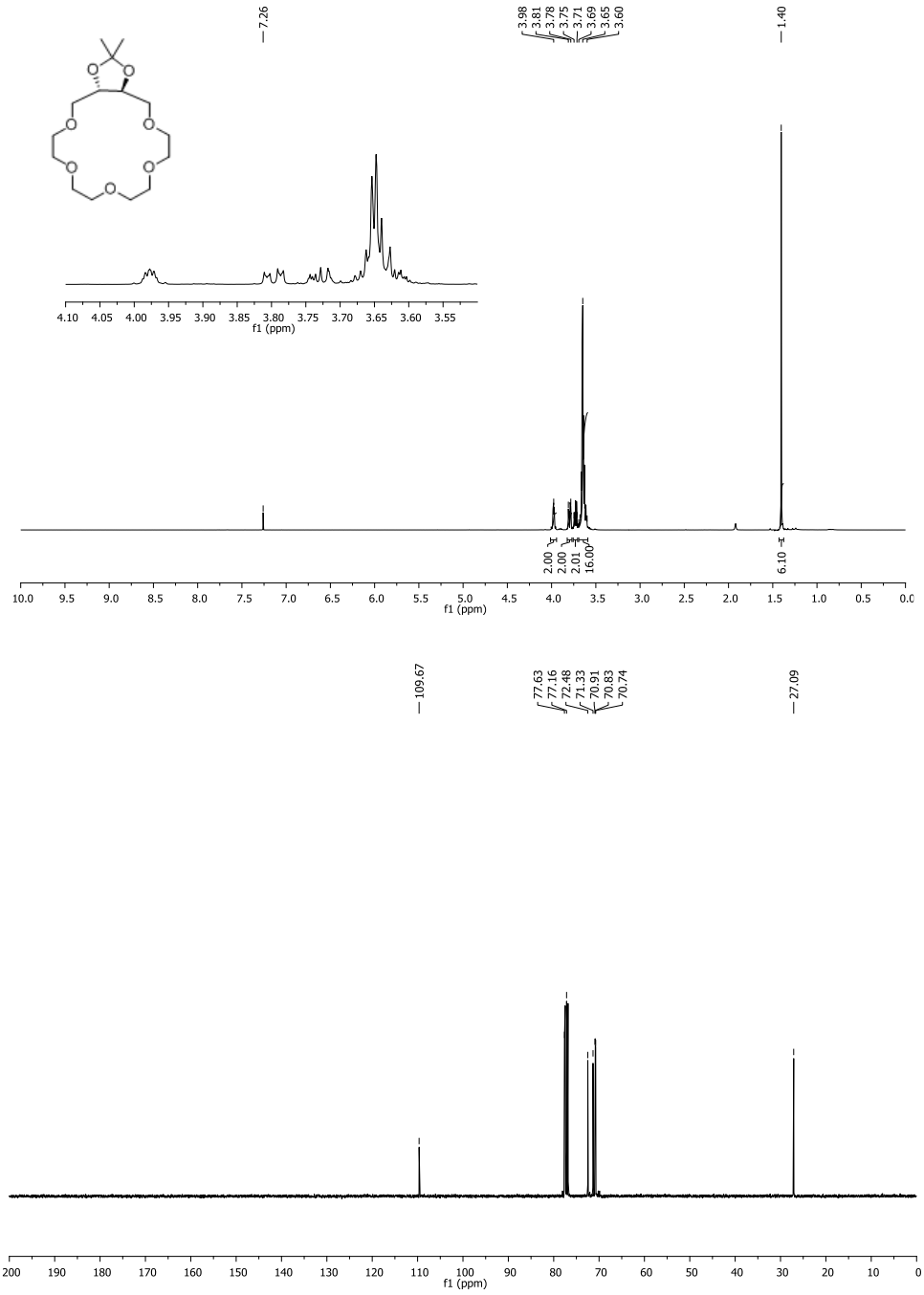

Supplementary Figure 1. ^{1}H NMR ($CDCl_3$; upper) and ^{13}C NMR ($CDCl_3$; lower) for **S1**.

(15*S*,16*S*)-1,4,7,10,13-Pentaoxacycloheptadecane-15,16-diol, S2

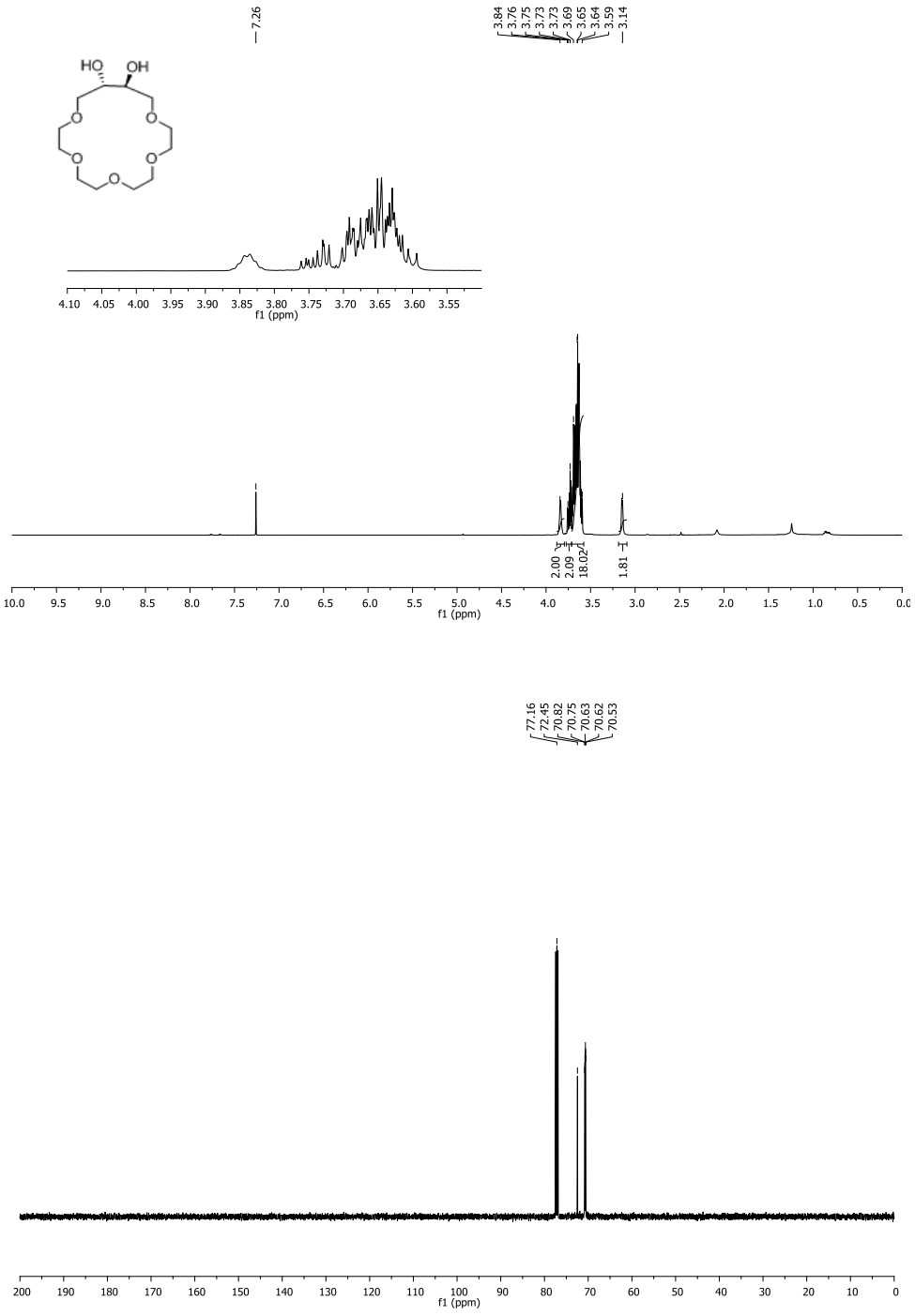

Supplementary Figure 2. ^{1}H NMR ($CDCl_3$; upper) and ^{13}C NMR ($CDCl_3$; lower) for **S2**.

(15*S*,16*S*)-1,4,7,10,13-Pentaoxacycloheptadecane-15,16-diyl dimethanesulfonate, S3

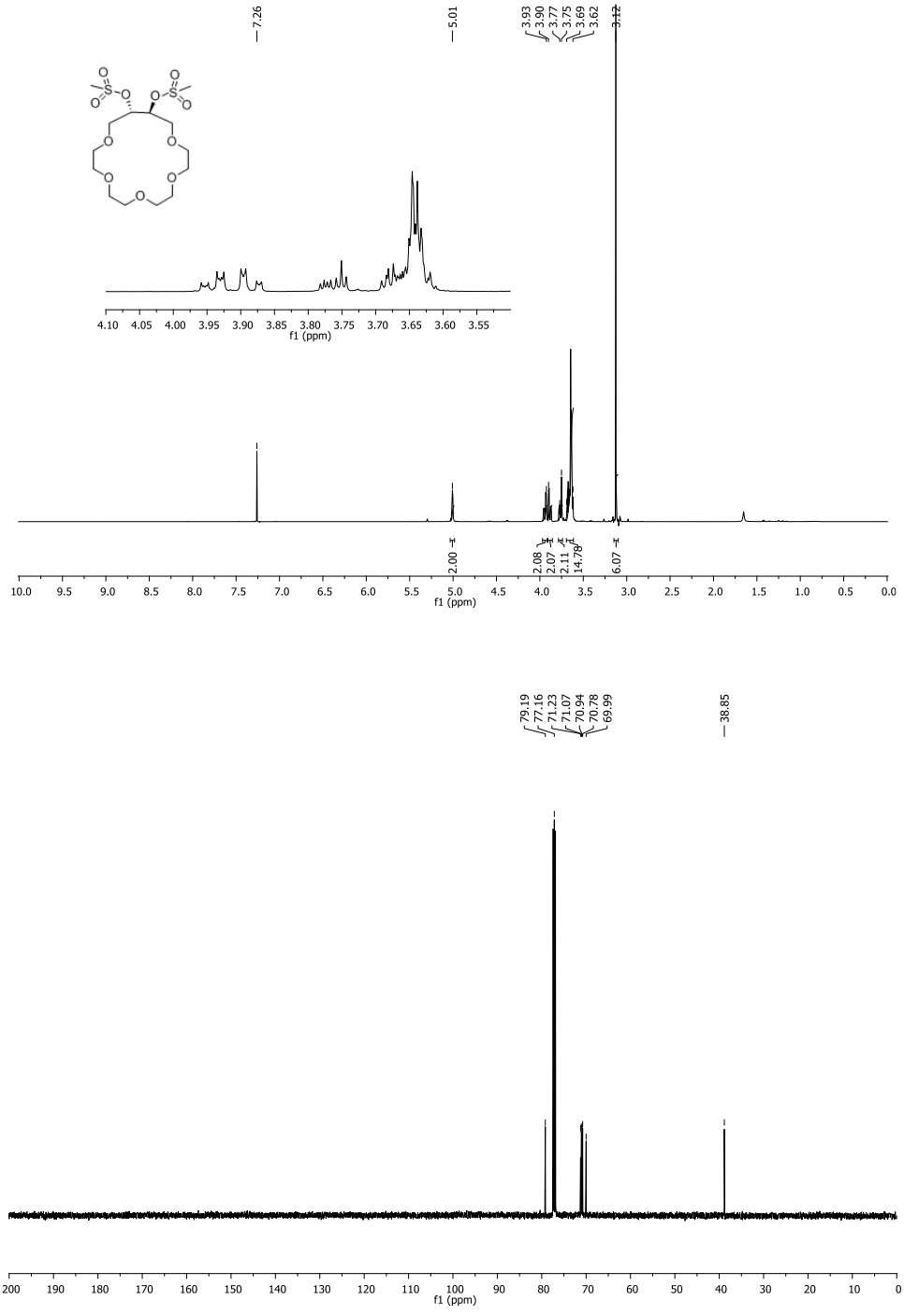

Supplementary Figure 3. ^{1}H NMR ($CDCl_3$; upper) and ^{13}C NMR ($CDCl_3$; lower) for **S3**.

(15*S*,16*S*)-15,16-Diazido-1,4,7,10,13-pentaoxacycloheptadecane, S4

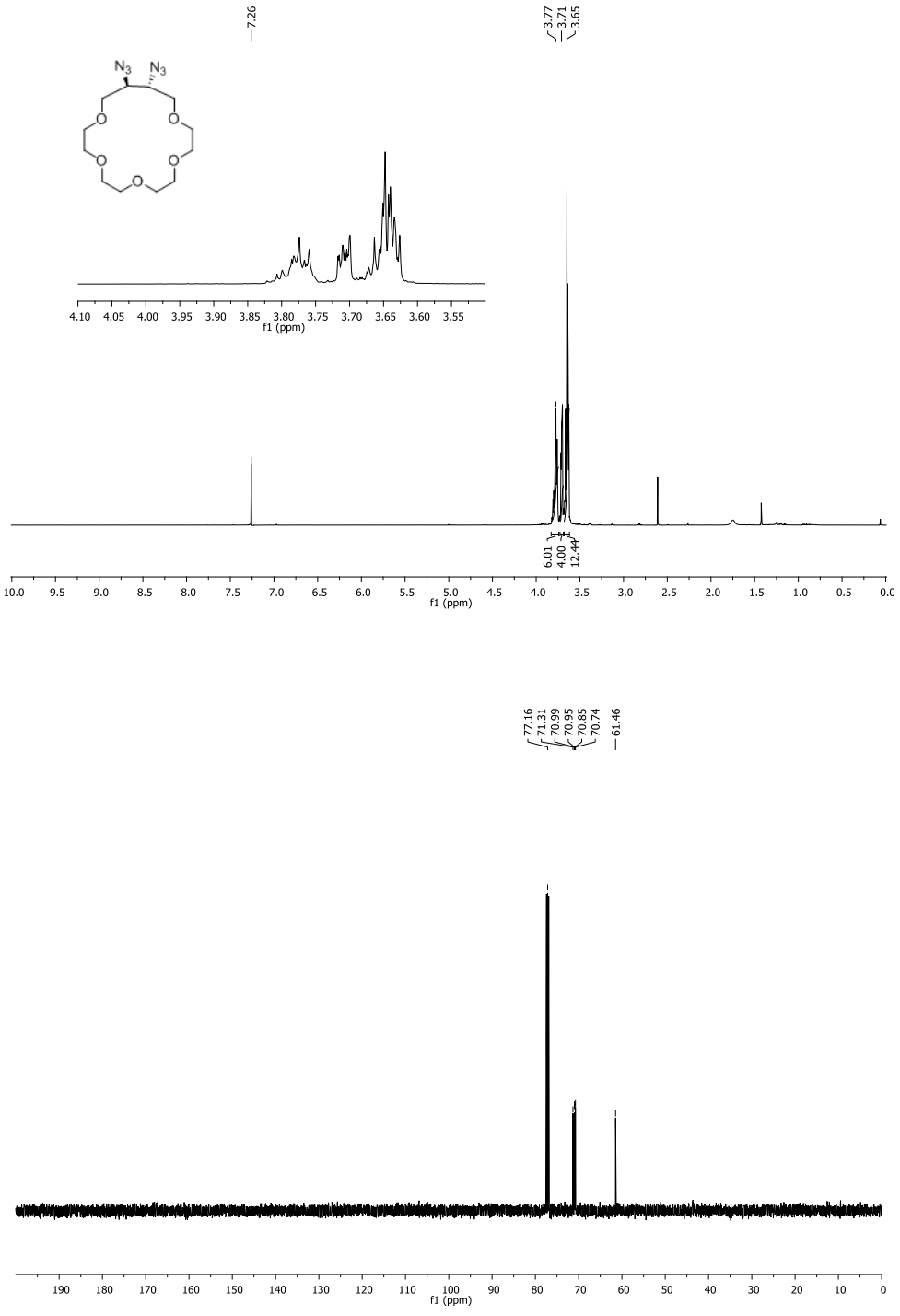

Supplementary Figure 4. ^{1}H NMR ($CDCl_3$; upper) and ^{13}C NMR ($CDCl_3$; lower) for **S4**.

(15*S*,16*S*)-1,4,7,10,13-Pentaoxacycloheptadecane-15,16-diamine, S5

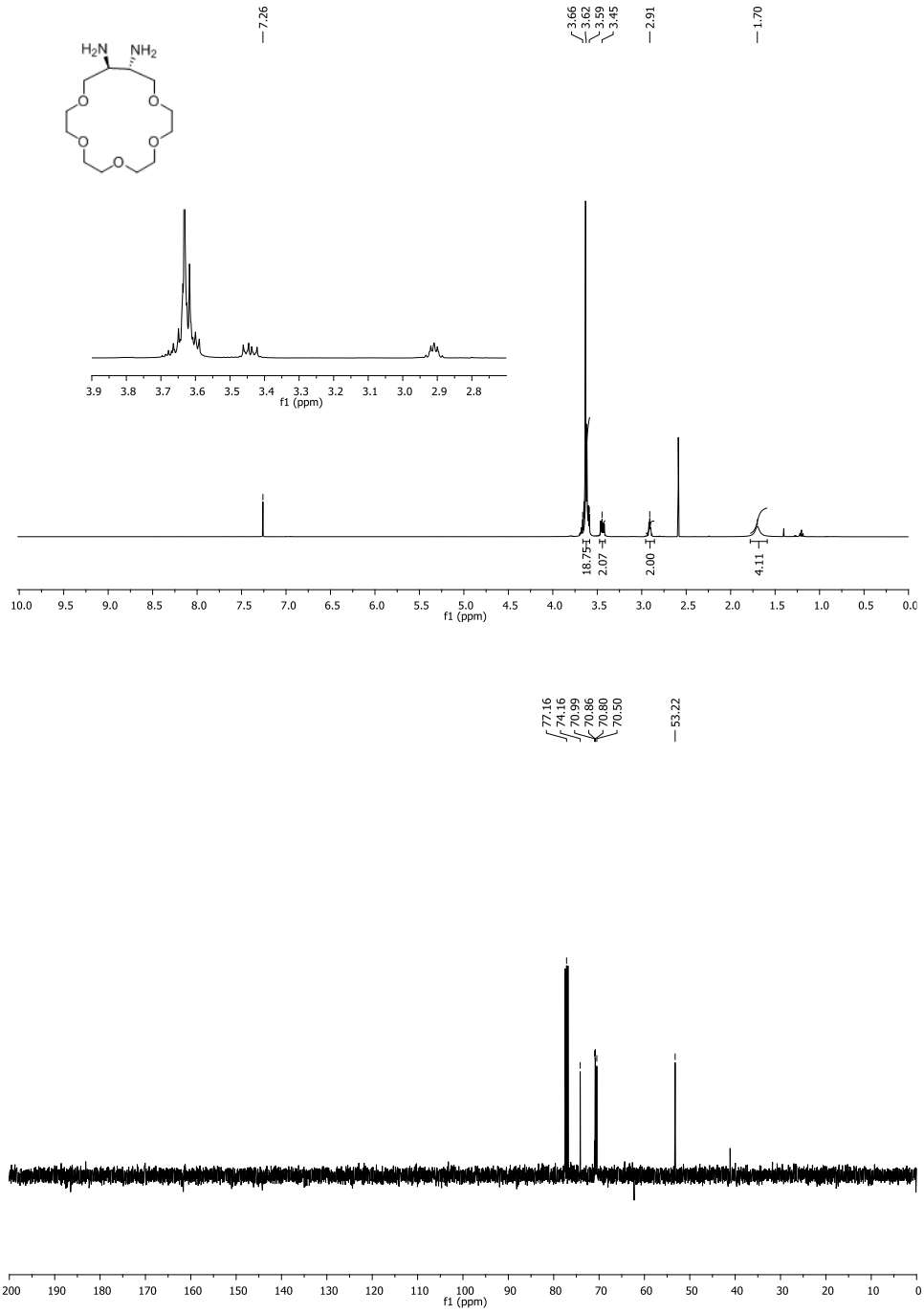

Supplementary Figure 5. ^{1}H NMR ($CDCl_3$; upper) and ^{13}C NMR ($CDCl_3$; lower) for **S5**.

2.3. Synthesis of the crown-ether cage

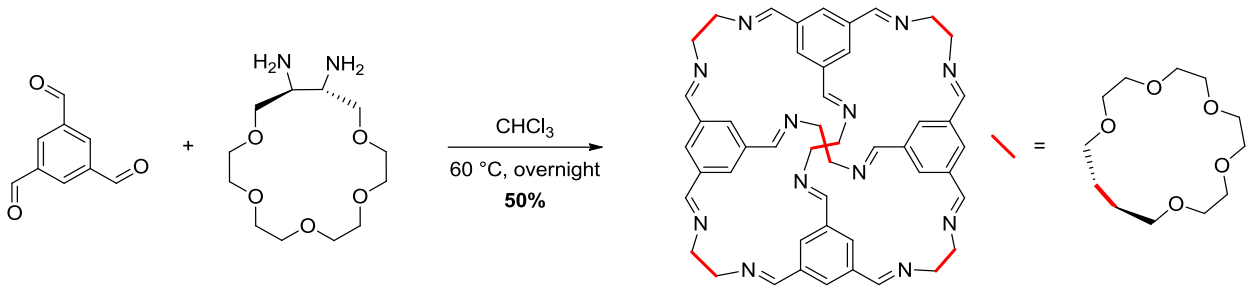

To a round bottom flask, equipped with stirrer bar, was added 1,3,5-triformylbenzene (200 mg, 1.23 mmol, 4.0 eq.) followed by a solution of diamine **S5** (686 mg, 2.46 mmol, 8.0 eq.) in $CHCl_3$ (7 mL). The resulting solution was heated at 60 °C under N_2 for 21 h, or until full conversion to the desired cage product had occurred, as determined by ^{1}H NMR analysis of crude aliquots. On completion, the reaction mixture was allowed to cool to RT before the solution was diluted with $CHCl_3$ (20 mL), dried (K_2CO_3), and then concentrated *in vacuo* to afford a thick, yellow oil. Isopropanol (10 mL) was added and the sample was then sonicated and gently heated until all the material had fully dissolved. The resulting yellow solution was left to cool and the pale yellow solid that precipitated was collected by filtration and dried under reduced pressure. The solid was then further dried in a vacuum oven at 40 °C overnight, and then at 60 °C for 4 h, to afford the desired cage product as a pale, yellow solid (326 mg, 0.155 mmol, 50 %).

Mpt decomposes >180 °C; **IR** (ν_{max}/cm^{-1}) 2858, 1649, 1598, 1445, 1352, 1298, 1250, 1111, 978, 943, 882; **^{1}H NMR** (500 MHz, $CDCl_3$) δ_H 8.12 (12H, s), 7.92 (12H, s), 4.03 (12H, d, J = 7.0 Hz), 3.75–3.58 (120H m); **^{13}C NMR** (126 MHz, $CDCl_3$) δ_C 161.06, 136.56, 130.20, 73.25, 72.68, 71.70, 71.09, 70.87, 70.60; **HRMS** (ES+) calc. for $C_{108}H_{156}N_{12}Na_2O_{30}$ $[M+2Na]^{2+}$ 1073.5422, found 1073.5496; **CHN Analysis** calc. for $C_{108}H_{156}N_{12}O_{30}$: C, 61.70; H, 7.48; N, 7.99; found: C, 59.57; H, 7.34; N, 7,74.

2.4. NMR spectra of the crown-ether cage

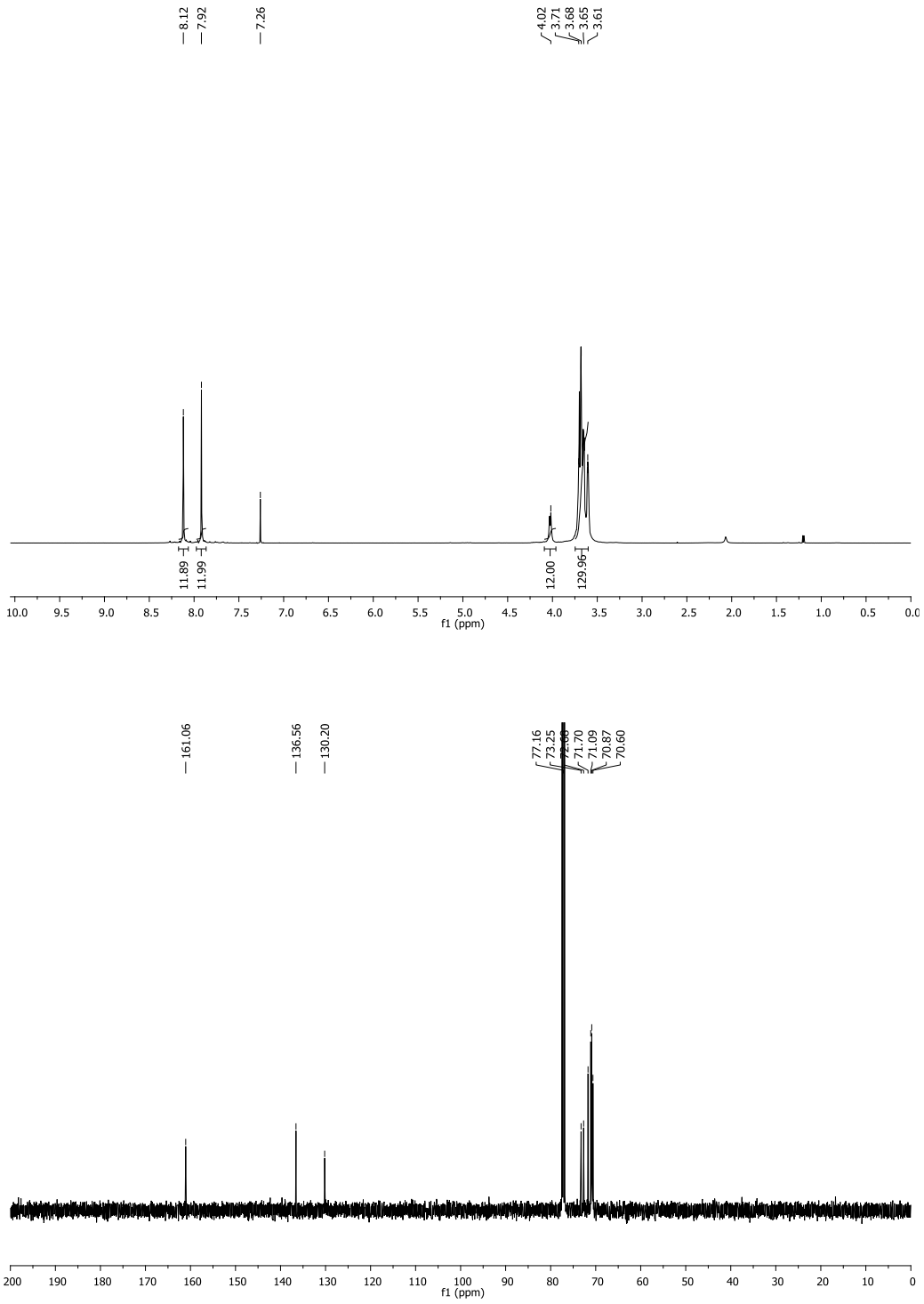

Supplementary Figure 6. ^{1}H NMR ($CDCl_3$; upper) and ^{13}C NMR ($CDCl_3$; lower) for the crown-ether cage.

2.5. QTOF-MS of the crown-ether cage

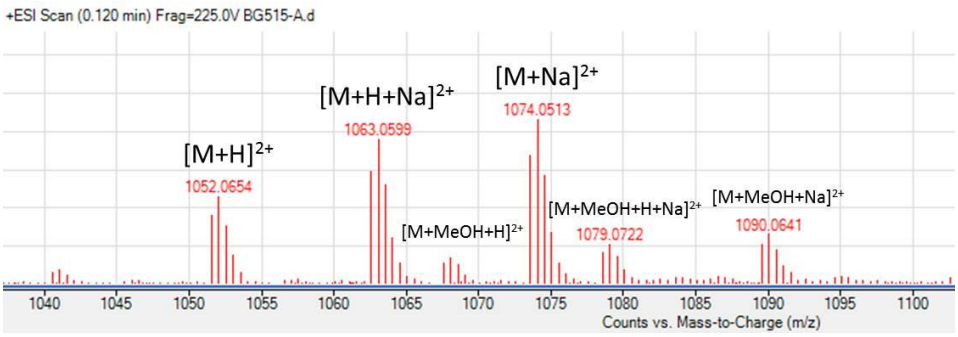

Supplementary Figure 7. QTOF mass spectrometry for the crown-ether cage.

2.6. HPLC analysis of the crown-ether cage

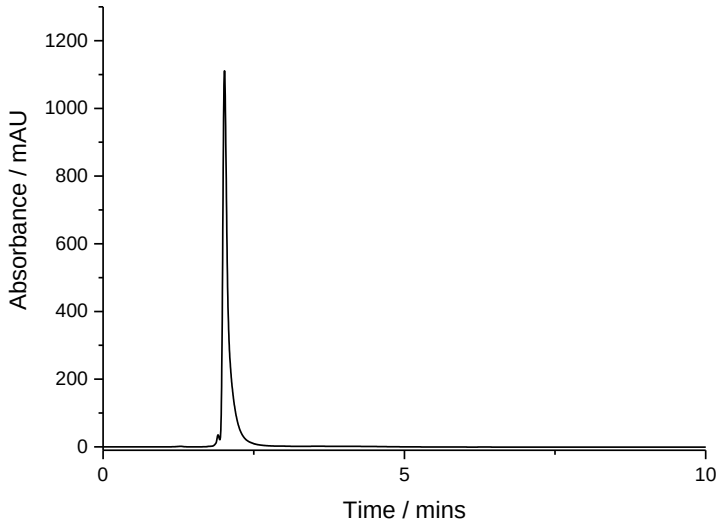

Supplementary Figure 8. HPLC analysis for the crown-ether cage

2.7. Preparation of the porous liquid using the crown-ether cage

The crown-ether cage (100 mg, 0.0475 mmol, 1.0 eq.) was dissolved in 15-crown-5 (113 μL, 0.5707 mmol, 12.0 eq.) by sonicating the mixture for 2 h to afford a viscous, pale yellow liquid.

2.8. Thermogravimetric analysis of the crown-ether cage and the porous liquid

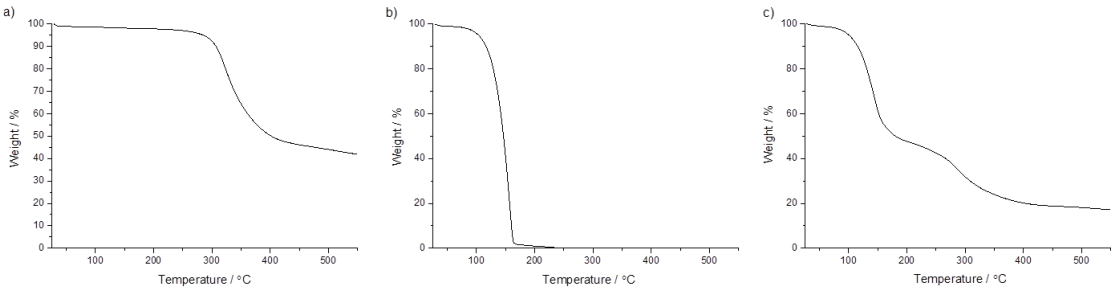

Supplementary Figure 9. TGA was conducted at a ramp rate of 5 °C/min up to 550 °C in an aluminium pan under a nitrogen flow for **a)** the crown-ether cage; **b)** 15-crown-5, and; **c)** the porous liquid (1:12 cage:15-crown-5).

2.9. Viscosity measurements for the porous liquid and for 15-crown-5 as a function of temperature

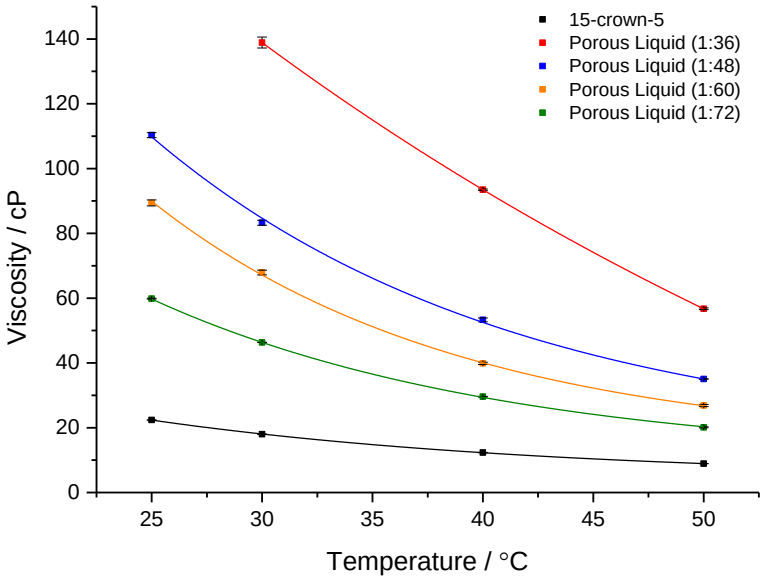

Supplementary Figure 10. Viscosity was measured as a function of temperature for a range of different porous liquid concentrations (given here as molar ratio of cage to crown-ether solvent), and for the neat crown-ether itself, 15-crown-5. All measurements were repeated three times with the average viscosity reported and the standard deviation displayed here as error bars.

2.10. Viscosity measurements for the porous liquid and for 15-crown-5 as a function of concentration

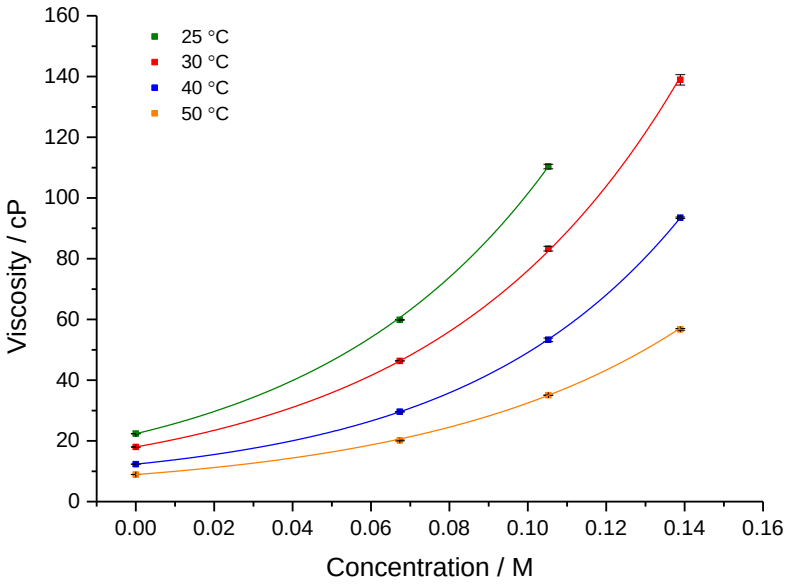

Supplementary Figure 11. The same viscosity data as in **Supplementary Fig. 10**, above, plotted as a function of molar crown-ether cage concentration at four different temperatures. Again, the standard deviation is displayed as error bars.

3. Molecular simulations for the crown-cage porous liquid

3.1. Models and force-fields

The molecular structure of the crown-ether substituted cage is shown in **Supplementary Figure 12a**. The six looped crown-ether moieties that decorate the cage are all identical, and they are structurally similar to the 15-crown-5 solvent that is used to provide fluidity in the porous liquid. Hence, the cage is designed to have high solubility in 15-crown-5. For visualisation purposes, and to emphasise the cage core, **Supplementary Figure 12b** shows the same molecule without any hydrogen atoms. The pseudo-octahedral structure of the cage core is highlighted using yellow glyphs. Henceforth, we will refer to the crown-ether cage molecule as the "crown cage", and to the 15-crown-5 solvent molecule as the "solvent".

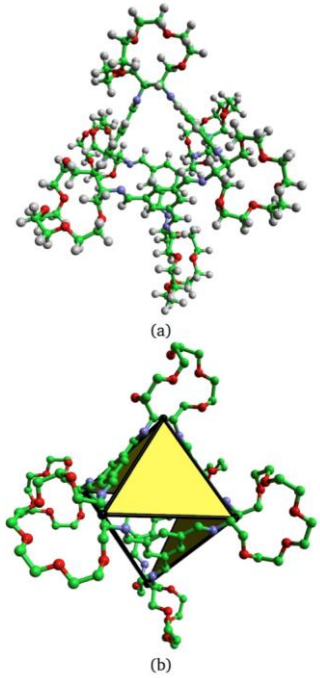

Supplementary Figure 12. The cage core is decorated with six crown-ether moieties. **a**, Crown cage molecule with all atoms shown. **b**, Octahedral representation of the crown cage molecule with hydrogen atoms removed for clarity. The access windows are highlighted by yellow glyphs with black outlines. In both **a** and **b**, double bonds (imines and aromatic) have been removed for clarity. Green spheres = carbon; red spheres = oxygen; grey spheres = hydrogen; blue spheres = nitrogen.

Atomistic models for the cage and solvent molecules were constructed using the OPLS all atom force-field[2,3]. This force-field considers every atom of the molecule explicitly. The model parameters for the crown cage molecule were constructed from a single irreducible unit, as depicted in **Supplementary Figure 13a**. This unit is connected to three other identical moieties to form the molecular structure. Identifying all the atom types within this single repeating unit is enough to specify all the atom types in the whole cage molecule. As a visual aid, **Supplementary Figure 13b** shows a decorating crown-ether moiety in its entirety, attached to a cage vertex. Also, **Supplementary Figure 13c** shows the all atom representation of a solvent molecule. The only difference between this molecule and the crown ether groups that functionalise the cage is the presence of the two bridging carbons at the vertex of the cage core. This increases the size of the crown-ether ring. Force-field parameters for all these molecules are provided in **Supplementary Tables 4–7**.

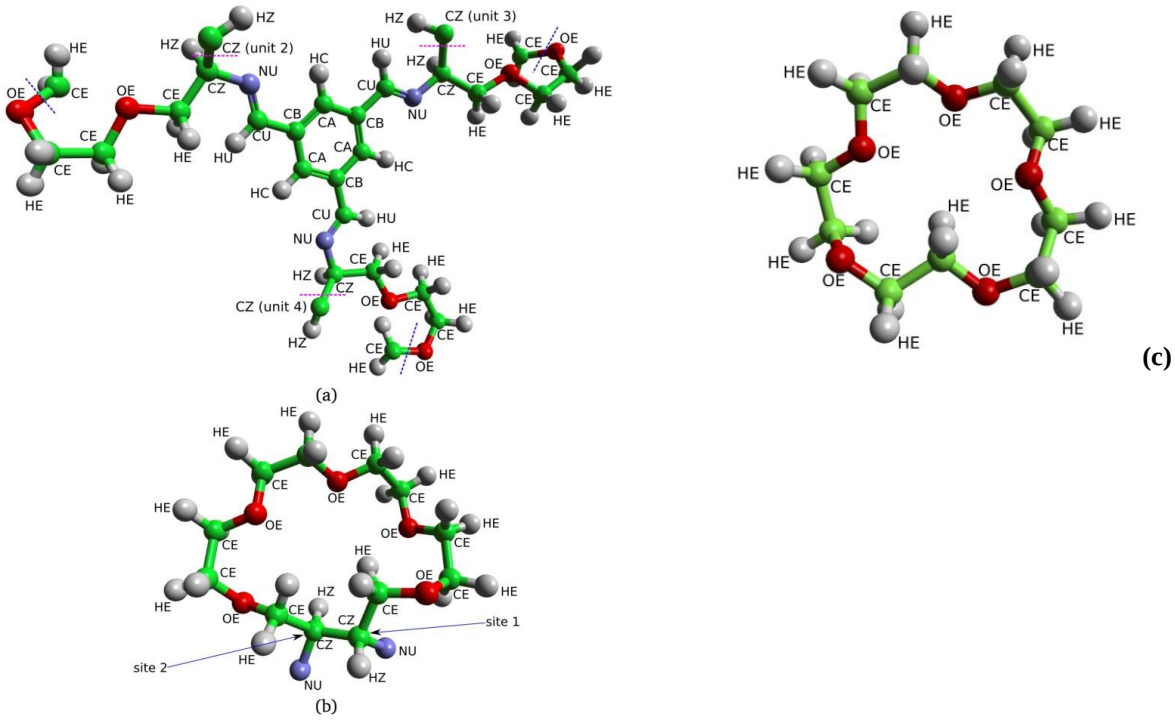

Supplementary Figure 13. **a**, Repeating unit for the crown cage molecule. Green spheres denote carbon atoms, blue spheres denote nitrogen, grey spheres denote hydrogen, and red spheres denote oxygen. Pink dashed lines at CZ groups denote a connection to another identical unit and blue dashed lines at CE groups denote connections to the rest of the crown ether moiety at that vertex. **b**, Crown cage moiety with its two termini attached to the vicinal carbons on the cage vertex. The parameters for the atom types are given in Supplementary Table 4. **c**, All atom model of a 15-crown-5 solvent molecule. Notice the similarity between this molecule and its cage-attached analogue in panel **b**.

3.2. Free energy calculations

Before carrying out bulk molecular dynamics (MD) simulations for the porous liquid, we computed the free energy cost for introducing a single 15-crown-5 molecule into the cage cavity. We used the Umbrella Sampling (US) method[4] combined with the Weighted Histogram Analysis Method (WHAM)[5,6]. Given that solvent molecules are very similar to the looped moieties decorating the cage cores (**Supplementary Figure 12**), this should also give an indication as to whether, in a bulk system, a looped moiety of one cage could occupy the cavity of a neighbouring

cage. The reaction coordinate for the free energy profile was defined as $q = \left| \mathbf{r}^c_1 - \mathbf{s}_1 \right|$, where $\mathbf{s}_1$ is the centre of mass of two adjacent carbon atoms in the 15-crown-5 molecule, and $\mathbf{r}^c_1$ is the centre of the crown cage (**Supplementary Figure 14a**).

The US simulations were performed with the GROMACS-4.5.3 code[7], in the canonical ensemble (NVT) at 400 K, and using a time-step of 0.001 ps. Note that these simulations were performed with the two tagged molecules in vacuum, hence no periodic boundary conditions and no cut-offs were used. The restraining, or biasing, potential was of the form $V(q) = 0.5K(q-q_o)^2$. 97 US windows, with force-constants reported in **Supplementary Table 1**, were used to span the 0.0-5.04 nm interval. In each window, simulations were extended up to 50 ns, with the first 10 ns used as equilibration. The resulting free energy profile, shown in **Supplementary Figure 14b**, reveals that cage occupation by a solvent molecule is a highly unfavourable process. The minimum at approximately 0.80 nm corresponds to a configuration where the solvent molecule sits outside the cage window. Beyond this minimum, at closer distances to the cage centre, there is a sharp rise in the free energy, and a strongly repulsive potential wall is observed. There is no minimum in the free energy profile for any configuration where the reference point of the solvent is inside the cage cavity. This indicates that cage occupation by a solvent molecule, or a pendant crown-ether moiety of another cage, is highly unfavourable due to steric effects.

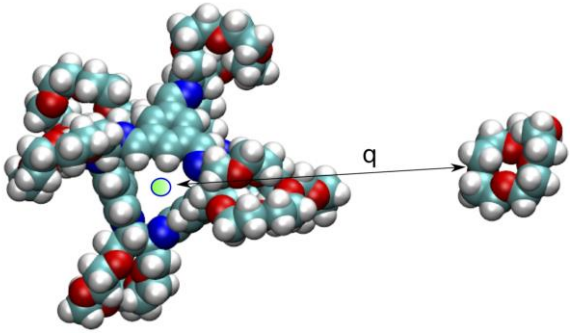

(a)

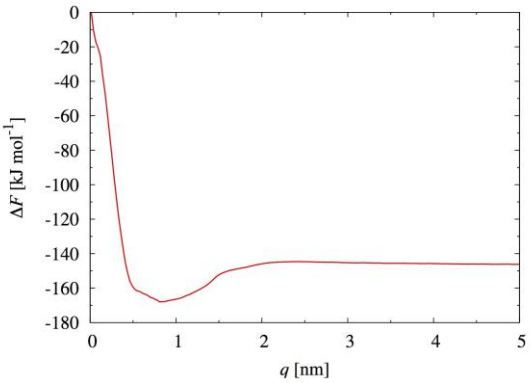

(b)

Supplementary Figure 14. Free energy calculations. a, Reaction coordinate, q, for the potential of mean force to force a solvent molecule into the centre of a crown cage cavity at 400 K. **b**, Helmholtz free energy profile for the occupation of a single crown cage molecule by a solvent molecule at 400 K.

Supplementary Table 1 Umbrella Sampling window parameters for the crown cage and solvent PMF.

Range [nm]	Nº of windows	Interval between windows [nm]	K [kJ mol^{-1} nm^{-2}]
0.00 – 0.78	40	0.02	250000
0.80 – 1.12	8	0.04	5000
1.20 – 5.04	49	0.08	1000

3.3. Molecular dynamics simulations for the porous liquid

MD simulations of a bulk system were run on a sample consisting of 40 cages and 480 solvent molecules enclosed in a cubic and periodic simulation box, reproducing the 1:12 molar ratio of cage to solvent used in the experiments. Molecular Dynamics (MD) simulations were run in the isobaric-isothermal ensemble (NPT), using a time-step of 1 fs. The NPT ensemble conditions were imposed by combining a Nose-Hoover thermostat[8,9] and a Parrinello-Rahman barostat[10], with time constants of 0.1 ps and 1 ps, respectively. Lennard-Jones interactions were cut off at 1.4 nm, while Coulomb forces were computed using the smooth particle mesh Ewald technique[11]. A relative strength of 10^{-5} was used for the Ewald-shifted direct potential at 1.7 nm, together with a set of k-vectors with a maximum length of 15 in reciprocal space. Bond constraints were imposed on all bonds involving hydrogen atoms. Starting configurations were equilibrated at high temperature, and systems were then annealed from 600 K to 200 K, at a constant rate of 4 K/ns and a pressure of 1 bar. Configurations sampled along the annealing trajectory were used as starting points for 100 ns-long NPT trajectories at T = 400 and 350 K. **Supplementary Figure 15a** illustrates the molecular packing in the simulation box. The atoms of the solvent molecules are represented by translucent spheres to show their larger numbers in comparison with the atoms of the crown cage molecules (opaque spheres). In **Supplementary Figure 15b**, all solvent molecules and crown ether moieties are represented by lines to allow visualisation of the cage cores, which are again represented as opaque spheres. For comparative purposes, we also set up a bulk simulation of the pure 15-crown-5 ether solvent, which was also annealed from 600 K and run for 100 ns at 400 K, 350 K and P = 1 bar. The solvent sample consisted of 500 molecules. The MD control parameters were the same as used for the 1:12 mixture, and are summarized in **Supplementary Table 2**.

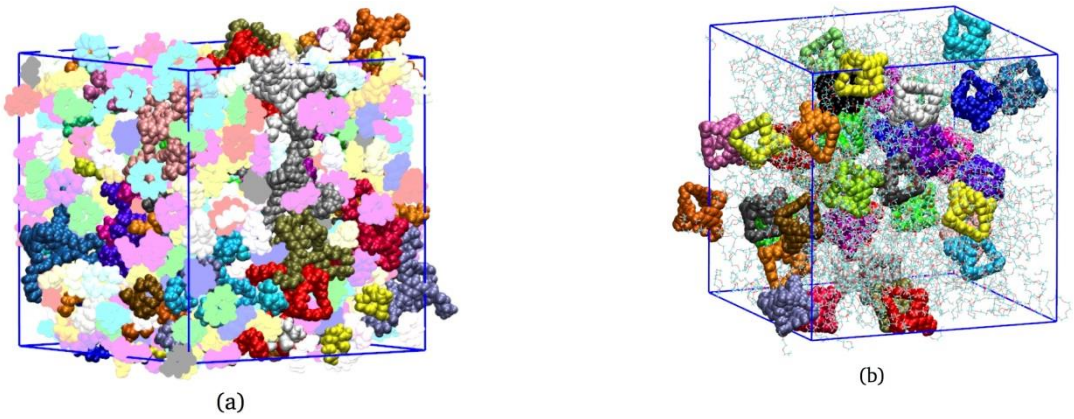

Supplementary Figure 15. Molecular dynamics simulations. Sample configuration of the bulk porous liquid; both figures represent the same configuration. **a**, The atoms of each crown cage molecule are represented as opaque spheres of the same colour. The atoms of the solvent molecules are represented with translucent spheres of the same colour. **b**, To highlight the distribution of the cage molecules, all looped moieties and solvent molecules are drawn with lines of the appropriate colour. The cage cores are highlighted by representing their atoms as opaque spheres of the same colour.

Supplementary Table 2 Standard input parameters used for the NPT MD simulations run with GROMACS-4.5.3

Input Parameter	**Value**
Time step	1 fs
Cut-off (Lennard-Jones)	1.4 nm
Real-space cut-off (Coulomb)	1.7 nm
Thermostat time constant	0.1 ps
Barostat time constant	1.0 ps
Pressure	1.01325 bar
Fourier (nx, ny, nz)	15
Ewald-rtol	10^{-5}

In order to probe the liquid structure of the mixture, the following radial distribution functions (RDF) were computed:

- The cage–cage RDF, $g_c(r)$, computed from the cage centres.
- The cage–solvent RDF, $g_{cs}(r)$, computed from the centre of the cage and the centre of the solvent molecules
- The solvent–solvent RDF, $g_s(r)$, computed from the centre of the solvent molecules

Supplementary Figure 16 shows the three RDFs at 400 K and 350 K. The corresponding coordination numbers at 400 K are shown in the insets of these plots. From the cage-cage RDF, **Supplementary Figure 16a**, it is clear that two solvation shells are present in this system; one at 1.21 nm and the other at 1.82 nm. The first solvation shell is bifurcated, with one peak at 1.14 nm and the other at 1.26 nm. The coordination number, N(r) = 0.9, in this solvation shell suggests that, on average, the cage centres are coordinated by one other molecule, which is commensurate with a 1:12 molar ratio of cage to solvent. This also suggests the formation of dimers, as implied by **Supplementary Figure 16d**, which shows a simulation snapshot at 400 K. A careful analysis of the system configurations also reveals that cage molecules tend to assemble into chain-like structures. The formation of these chains, and more complex structural patterns, are probably the cause of the second strong peak in the cage-cage RDF at 1.82 nm. Supplementary Figure 9d also shows a slight thermal effect in $g_c(r)$, with the peaks becoming less well-defined at 400 K compared to those at 350 K. **Supplementary Figure 16b** shows three well-defined peaks in the cage-solvent RDF. The first peak at 0.78 nm is essentially a pre-peak. The coordination number in this shell, up to the first minimum at 0.91 nm, is 2. This suggests that, on average, two solvent molecules aggregate around each cage at this close distance. The second peak at 1.07 nm is the most well-defined, with a very deep minimum at 1.23 nm, and is indicative of a strong structural feature at this distance. This coordination shell can be regarded as the first solvation shell, and a N(r) value of 9.5 suggests that there are almost 10 solvent molecules, on average, coordinating each cage molecule.

The solvent–solvent RDF is shown in **Supplementary Figure 16c**. Again, the first shell is bifurcated to give two peaks, one at 0.66 nm and the other at 0.87 nm. The inset reveals that there

are, on average, 8 solvent molecules surrounding any other solvent molecule within this first solvation shell. The second solvation shell, at 1.32 nm, suggests there may be more complex structural aggregations between the solvent molecules. The increase in temperature from 350 K to 400 K seems to have little effect on the bulk structure of the solvent molecules. The green and brown dashed lines in **Supplementary Figure 16c** show the $g_s(r)$ of the pure solvent (no cage molecules) at 350 K and 400 K respectively. The striking similarity between these curves and the corresponding solvent-solvent RDF computed from the 1:12 mixture, suggests that the cages have little influence on the packing of the solvent molecules at these temperatures and at this concentration.

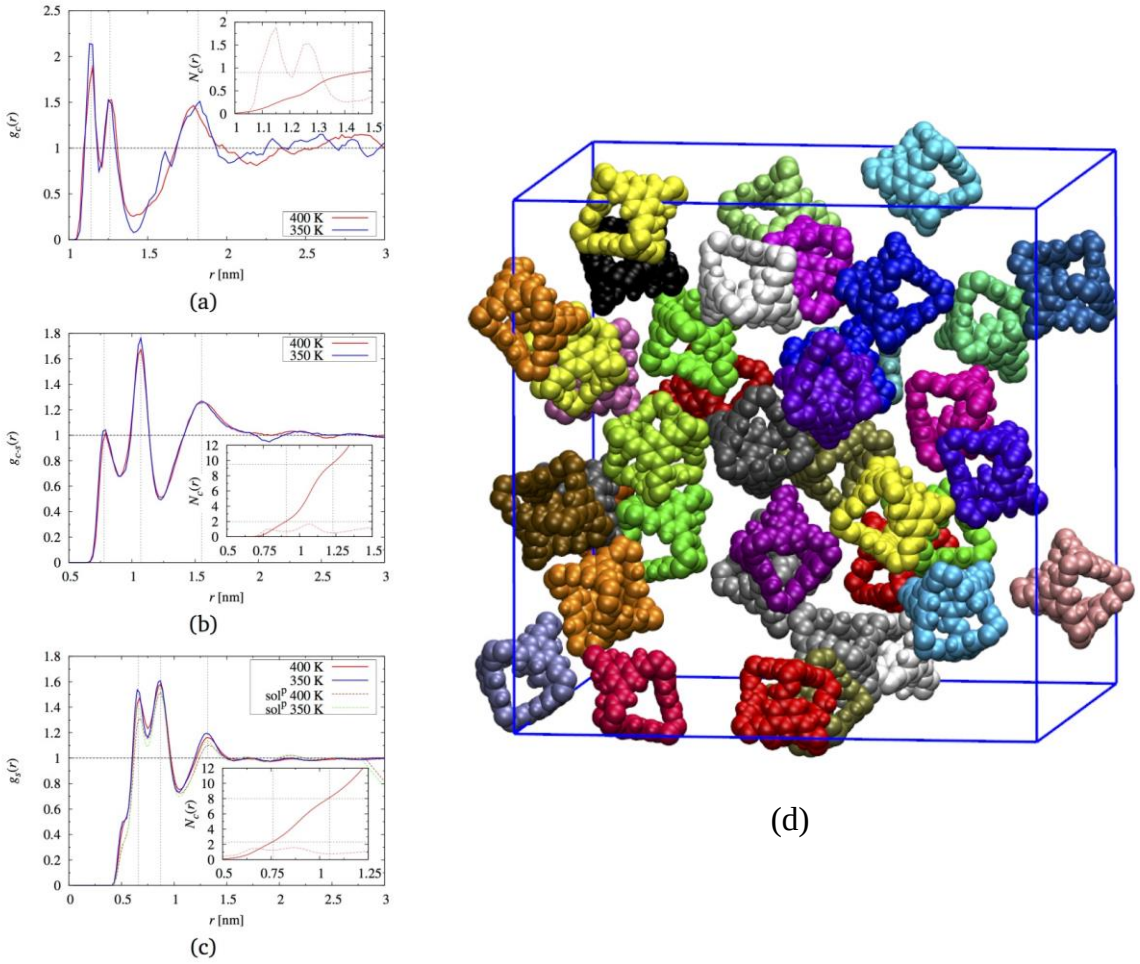

Supplementary Figure 16. Radial distribution functions for the 1:12 mixture at 400 K and 350 K. **a**, Cage–cage RDF, $g_c(r)$. **b**, Cage–solvent RDF, $g_{cs}(r)$. **c**, Solvent–solvent RDF, $g_s(r)$. The green and brown dashed lines in plot **c** show the $g_s(r)$ of the solvent molecules in the pure solvent at 350 K and 400 K, respectively. Insets: running coordination numbers, $N_c(r)$, $N_{cs}(r)$, and $N_s(r)$ at 400 K. The dashed vertical lines in the main plot show the location of the main peaks in the RDFs. Dashed black horizontal lines in the inset denote the coordination number at the corresponding minimum (black dashed vertical lines). The red dashed line in the insets shows the RDFs at 400 K from the corresponding main plot. **d**, Representative configuration of the 1:12 mixture at 400 K, highlighting structural aggregation. This snapshot reveals that some cages are aggregating as dimers. Only cage atoms are represented. The atoms of each cage are represented by opaque spheres of the same colour.

The mobility of the molecules in the 1:12 mixture, and in the pure solvent, was probed via the mean squared displacements of the geometric centre of the molecules. The corresponding diffusion coefficients are reported in Supplementary Table 3. Solvent molecules in the mixture are much more diffusive than cage molecules and, as expected, their mobility increases with increasing temperature. Also, the crown-ether molecules in the pure solvent are more mobile than in the cage–solvent mixture. In fact, at 350 K the molecules in the pure solvent are more diffusive than their 1:12 mixture-counterparts at 400 K. Therefore, the presence of the cages in the porous liquids hinders the mobility of the 15-crown-5 ether molecules. Nonetheless, at 350 K, simulations for this 1:12 mixture show clear signs of fluidity within the 100 ns simulation timescale.

Supplementary Table 3 Self-diffusion coefficients of molecules in the 1:12 mixture and in the pure solvent at 350 K and 400 K.

Species	T[K]	D[nm^2 ps^{-1}]
Cage	400	$5.86\ 10^{-7}$
Cage	350	$6.56\ 10^{-8}$
Solvent	400	$2.61\ 10^{-5}$
Solvent	350	$2.24\ 10^{-6}$
Pure Solvent	400	$2.60\ 10^{-4}$
Pure Solvent	350	$3.97\ 10^{-5}$

3.4. Cavity size distributions and relative porosity

The simulations discussed in the previous sections revealed that all cage cavities remain unoccupied, both at 350 K and 400 K. In other words, no atom of any solvent molecule, or looped moiety for a crown cage, is found to be inside in a cage cavity at any point; that is, at less than 0.275 nm from the cage centre. This is supported by the free energy profile in **Supplementary Figure 14b**, and it establishes the concept of permanent porosity in the liquid phase.

To examine the nature of the porosity in these systems, the distribution of cavity sizes in the liquid was computed in accordance with the theory and methods outlined by Pratt and Pohorille[12,13]. In particular, we used the so-called insertion probability, $\rho(R)$, which is defined as the likelihood that

a hard sphere solute of radius R could be located at an arbitrary point within the liquid without overlap with the van der Waals volume of any atom. This insertion probability is given by:

$$\rho = \frac{V(R)}{V_s}$$

where V(R) denotes the average volume accessible to such a solute, and V_s is the volume of the liquid sample. **Supplementary Figure 17a** shows the insertion probability, or fractional free volume, for the 1:12 cage–solvent mixture and for the pure solvent at 400 K and 350 K. For the pure solvent, these distributions display similar signatures to those computed by Pratt and Pohorille for simpler liquids[12,13]. Up to 0.03 nm, the insertion probability in the mixture is identical to the pure solvent, suggesting that the cage molecules have almost no influence on the fractional free volume accessible to small probes. At 350 K, the fractional free volume in the mixture is larger than for the pure solvent for probes with R > 0.03 nm, while at 400 K, the same behaviour is observed for R > 0.06 nm. The inset in **Supplementary Figure 17a** highlights the influence of the cage molecules on ρ(R) for values of R in the 0.1–0.17 nm range. The fractional free volume increases with increasing temperature, an effect that is more pronounced in the pure solvent.

Supplementary Figure 17b shows the insertion probability, $\rho_{ex}(R)=V_{ex}(R)/V_s$, which was calculated in the same way as ρ(R) but with blocking, or exclusion, of all the cage cavities. This was achieved by placing a hard-sphere of radius 0.25 nm at the centre of each cage core. For the sake of comparison, this figure also shows ρ(R) for the pure solvent. At 350 K, the two distributions are very similar, showing that it is equally likely to find a cavity of radius R in the crown ether solvent as in the intermolecular space of 1:12 mixture. At 400 K, the fractional free volume is slightly higher in the pure solvent in the space in the cage–solvent mixture with blocked cage cavities. The inset of **Supplementary Figure 17b** highlights this behaviour in the 0.1–0.17 nm range.

To assess the contribution from the cage cavities to the effective porosity of the mixture, we define the "relative porosity" of the mixture as:

$$V_{rel}(R) = \frac{\rho_{mix}(R)}{\rho_{sol}(R)}$$

where ρ_{mix} is the insertion probability in the mixture, and ρ_{sol} is the corresponding distribution for the pure solvent. In other words, V_{rel} is the ratio of insertion probabilities in the mixture and pure solvent at the same temperature. **Supplementary Figure 17c** shows $V_{rel}(R)$ at 350 K and 400 K, while the inset shows an expansion of the 400 K data. At this temperature, the cage cavities make a significant contribution to the fractional free volume of the mixture; indeed, at R ~ 0.25 nm (the effective cage-cavity radius), $\rho_{mix}(R)$ is thirty times larger than $\rho_{sol}(R)$. For values of R smaller than ~0.1 nm, V_{rel} is approximately 1, indicating that it is equally likely to insert a small spherical probe in the cage–solvent mixture and the pure solvent. At the tail end of the distribution, $V_{rel}(R)$ becomes less than unity, indicating that spontaneous thermal cavities with R > 0.275 nm are more likely to be found in the pure solvent. Clearly, there is a smaller probability of inserting larger spherical probes in the finite and rigid cavity of the cage, and we would expect larger, low-curvature molecules to be totally size-excluded, as are the crown-ether moieties on the periphery of the cage. This opens up possibilities, for example, in size-selective extraction processes.

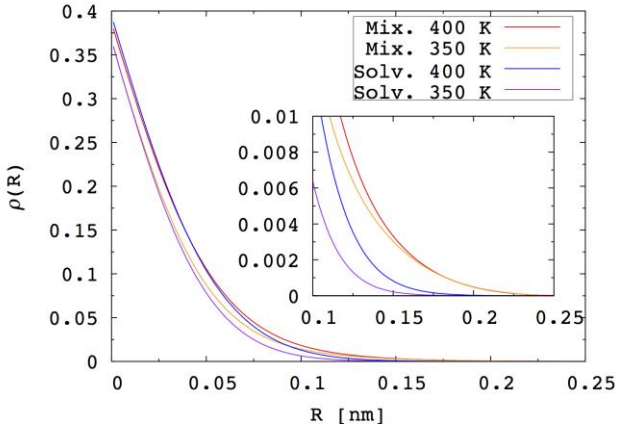

(a)

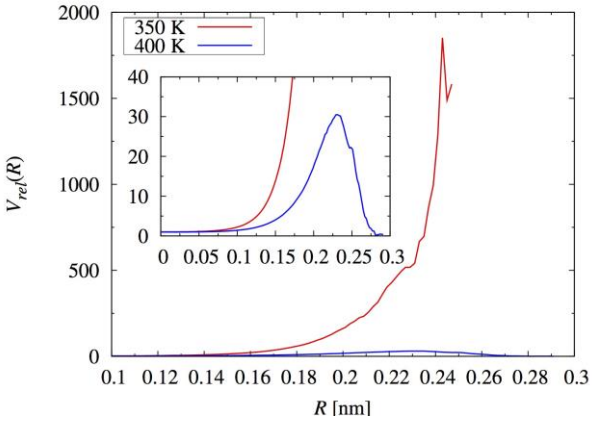

(c)

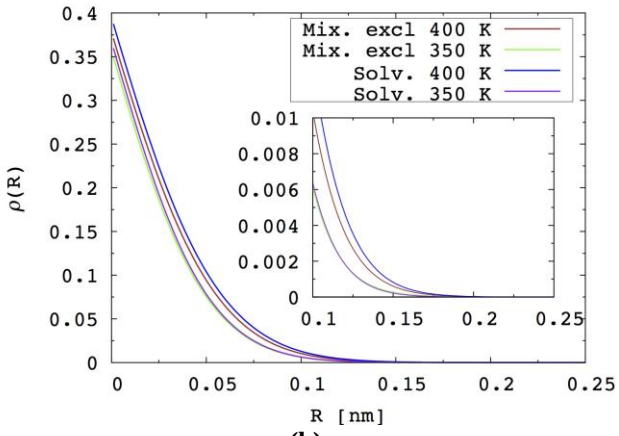

(b)

Supplementary Figure 17. Insertion probabilities, ρ(R), for the 1:12 porous liquid and the pure solvent at 350 K and 400 K. a, The mixed system compared with the pure solvent, considering the contribution from the cage cores. **b**, The mixed system compared with the pure solvent, neglecting the contribution from the cage cores. The insets show the distributions, ρ(R), over the range 0.1 to 0.25 nm. **c**, Relative porosity, $V_{rel}(R)$, of the 1:12 mixture at 350 K and 400 K. The inset focuses on the 400 K data.

Supplementary Figure 17c shows that there is a dramatic increase in relative porosity at 350 K. At R ~ 0.24 nm, the presence of the cage cores make the 1:12 mixture 1750 times more porous than the solvent at the same temperature. V_{rel} at 400 K is also shown in the main plot to illustrate

how much the relative porosity increases when the temperature decreases from 400 K to 350 K. Unlike the 400 K case, there is no sampling of cavities with R > 0.25 nm in the pure solvent at 350 K. We would assume that the decrease in temperature has no significant effect on the size of the intrinsic cage cavity because the cage core is fairly rigid, and no such temperature change is seen for solid, crystalline cages. Hence, the main plot in **Supplementary Figure 17c** suggests that there is significantly less fractional free volume accessible in the solvent at 350 K than there is 400 K. Moreover, close inspection of simulation snapshots suggests that there is more interstitial space between the molecules in the pure solvent at 400 K than at 350 K. In other words, molecular packing in the pure solvent is tighter at 350 K, limiting the size of the interstitial voids. This is accompanied by a 4.6 % increase in the solvent density, from 1022 Kg m^{-3} at 400 K to 1069 Kg m^{-3} at 350 K. Such reduction in interstitial void volume is only significant for cavities greater than 0.1 nm (see inset). The contribution from the cage cores is again maximised for probes radii of 0.23–0.24 nm.

3.5. Molecular dynamics simulations of the porous liquid saturated with methane

To assess the effect of the intrinsic porosity in the cages on the behaviour of small guest molecules, we carried out a simulation of the 1:12 mixture (again, 40 cage and 480 solvent molecules) combined with 100 methane molecules. The all atom force-field parameters for methane are provided in **Supplementary Tables 8–10**. The starting configuration was generated by randomly placing 100 methane molecules in the bulk fluid, avoiding atomic overlaps. The system was then relaxed for 75 ns under NPT conditions, and the production run consisted of a second 75 ns-long NPT trajectory at T=350 K and P = 1 bar. Again, bonds involving hydrogen atoms were constrained, and the MD parameters were those reported in **Supplementary Table 2**. The number of cages occupied by methane molecules and the number of methane molecules occupying cage cavities were monitored during the simulation. A methane molecule was considered to be 'inside' a cage when the distance between its carbon atom and the geometric centre of the cage-core was less than 0.275 nm.

Supplementary Figure 18 shows the number of occupied cages and the number of occupying methane molecules in the mixture as a function of time during the production run at 350 K. Note that the quantities plotted in the graph are system specific; there are 40 crown-cage molecules, 480 crown-ether solvent molecules, and 100 methane molecules in the simulation box (see snapshot,

Supplementary Figure 19). The methane molecules quickly occupied all 40 cages. The small fluctuations in the number of occupied cages (blue line) might lead one to conclude that the dynamics of cage occupation by methane is relatively slow, or that the methane molecules generally stay put once they are inside a cage cavity. The fluctuations in the number of occupying methane molecules show that this is not the case. Out of 100 methane molecules there are, on average, 60 methane molecules occupying 40 cages at any one time, suggesting that there is, on average, more than one methane molecule per cage at any time. The occupation/de-occupation dynamics are, in fact quite, fast.

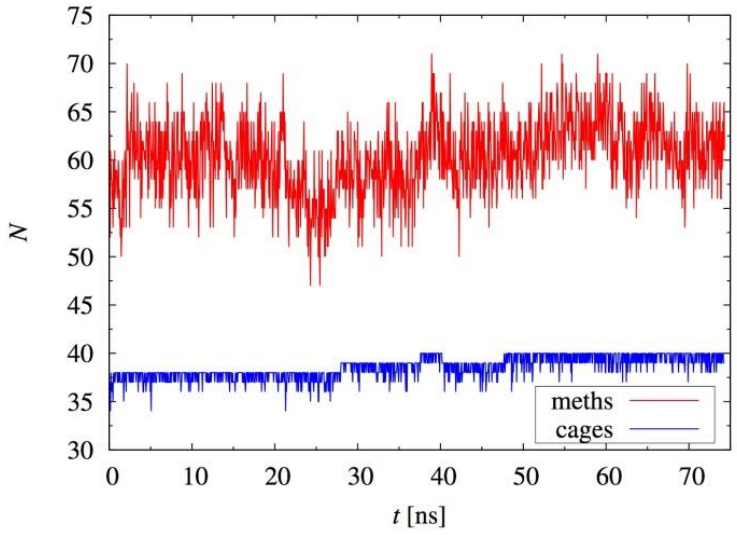

Supplementary Figure 18. Molecular dynamics for the porous liquid saturated with methane. Occupation data for the combined methane and porous liquid system at 350 K; cages = number of occupied cages; meths = number of cage-occupying methane molecules. The label, *N*, on the y-axis denotes these quantities in both cases. Note that these numbers are system specific. In this system, there are 40 crown cage molecules, 480 crown ether solvent molecules, and 100 methane molecules.

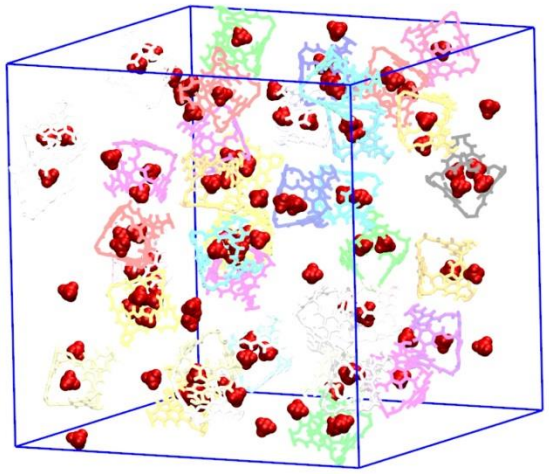

Supplementary Figure 19. Snapshot of the porous liquid with 100 methane molecules at 350 K. A simple bonding representation is used for the cage cores. Methane atoms are depicted using red spheres. Notice that all cage molecules are hosting at least one methane molecule. In some cases, there are as many as 4 methane molecules residing in one cage cavity. Crown-ether solvent molecules and crown ether cage substituents have been omitted for clarity.

3.6. Grand canonical Monte Carlo calculation of methane gas solubility in the porous liquid

In the previous simulations, the number of methane molecules dissolved in the mixture was fixed arbitrarily at the start and remained constant throughout the simulation. To probe likely methane solubility in the porous liquid, grand canonical Monte Carlo (GCMC) simulations were performed at 350 K, and at a chemical potential corresponding to the ideal-gas pressure of 1 bar. In these stochastic simulations, methane molecules are randomly inserted or removed from the system according to the acceptance criteria used to sample the Grand Canonical ensemble[4]. Given that the large cage molecules display slow dynamics at low temperatures, canonical moves (intramolecular moves, and molecular translations and rotations) lead to a very large rejection rate. Consequently, only grand canonical moves were considered in the simulations; that is, the insertion and deletion of gas molecules. A sample of 20 static configurations was drawn from the 100 ns MD trajectory of the 1:12 cage–solvent mixture at 350 K. For each configuration, the average number of methane molecules dissolved in the liquid was computed by GCMC, distinguishing between molecules

located inside and outside the cage cores. Each simulation consisted of 3.0×10^6 MC steps, which proved to be enough to equilibrate the concentration of gas in the system, followed by a production run of 6×10^6 MC steps. A similar procedure was repeated for the pure solvent.

The resulting equilibrium concentration of methane in the porous liquid was $X_{CH4} = N_{CH4}/(N_{CH4} + N_{Cages}) = 0.47$, with 70 % of the gas molecules occupying the built-in cavity of the organic cages. Alternatively, one can also compute the methane mole fraction in the porous liquid as $Y_{CH4} = N_{CH4}/(N_{CH4} + N_{Cages} + N_{Solvent}) = 6.38 \times 10^{-2}$, or the partial mole fraction $Z_{CH4} = N_{CH4}/(N_{CH4} + N_{Solvent}) = 6.88 \times 10^{-2}$. This latter quantity allows a clearer comparison with the solubility of methane in the pure solvent, which was found to be $Z_{CH4} = N_{CH4}/(N_{CH4} + N_{Pure\text{-}Solvent}) = 1.9 \times 10^{-3}$.

Although the calculated methane solubility is very close to the experimental values reported in the manuscript, the level of agreement between simulation and experiment is probably fortuitous, given that the calculation of low solubilities from Grand Canonical Monte Carlo simulations is prone to large finite size effects. Nonetheless, our simulations results clearly demonstrate that the empty intramolecular cavities in the porous liquid increases the solubility of methane with respect to the pure solvent by more than one order of magnitude, as found by experiment.

3.7. Forcefield parameters

Supplementary Table 4. Atom type parameters for cage molecules and pure solvent

Atom Type	Mass	Charge [e]	σ [nm]	ε [kJ mol^{-1}]
CB	12.011	0.000	0.3550	0.2929
CA	12.011	-0.115	0.3550	0.2929
HC	1.008	0.115	0.2420	0.1255
CU	12.011	0.246	0.3500	0.3347
HU	1.008	0.045	0.2500	0.2092
NU	14.007	-0.598	0.3250	0.7113
CZ	12.011	0.313	0.3500	0.2761
HZ	1.008	-0.006	0.2500	0.1255
CE	12.011	0.140	0.3500	0.2761
HE	1.008	0.030	0.2500	0.1255
OE	15.999	-0.400	0.2900	0.59

Supplementary Table 5. Bond stretching parameters for cage molecules and pure solvent

Bond Type	k_r [kJ mol^{-1} nm^{-2}]	r_{eq} [nm]
CA-HC	307105.6	0.1080
CB-CA	392459.2	0.1400
CE-CE	224262.4	0.1529
CE-CZ	224262.4	0.1529
CE-HE	284512.0	0.1090
CE-OE	267776.0	0.1410
CU-CB	357313.6	0.1481
CZ-CZ	224262.4	0.1529
CZ-HZ	284512.0	0.1090
CZ-NU	282001.6	0.1451
HU-CU	307105.6	0.1080
NU-CU	442667.2	0.1250

Supplementary Table 6. Bond bending parameters for cage molecules and pure solvent

Angle Type	k_θ [kJ mol^{-1} rad^{-1}]	θ_{eq} [^{o}]
CA-CB-CA	527.18	120.0
CB-CA-CB	527.18	120.0
CB-CA-HC	292.88	120.0
CE-CE-OE	418.40	109.5
CE-CZ-CZ	488.27	112.7
CE-CZ-HZ	313.80	110.7
CE-CZ-NU	418.40	109.0
CE-OE-CE	502.08	109.5
CU-CB-CA	585.76	120.0
CZ-CZ-NU	418.40	109.0
CZ-NU-CU	585.76	119.4
HE-CE-CE	313.80	110.7
HE-CE-CZ	313.80	110.7
HE-CE-HE	276.14	107.8
HE-CE-OE	292.88	109.5
HU-CU-CB	292.88	115.1
HU-CU-NU	292.88	123.2
HZ-CZ-CZ	313.80	110.7
NU-CU-CB	585.76	120.0
NU-CZ-HZ	292.88	109.5
OE-CE-CZ	418.40	109.5

Supplementary Table 7. Dihedral potential parameters for cage molecules and pure solvent

Dihedral Type	C_1 [kJ mol^{-1}]	C_2 [kJ mol^{-1}]	C_3 [kJ mol^{-1}]	C_4 [kJ mol^{-1}]
CA-CB-CA-HC	0.000	30.334	0.000	0.000
CA-CB-CU-HU	0.000	30.334	0.000	0.000
CB-CA-CB-CA	0.000	30.334	0.000	0.000
CE-CZ-CZ-CE	5.439	-0.209	0.837	0.000
CE-CZ-CZ-HZ	0.000	0.000	1.255	0.000
CE-CZ-CZ-NU	10.008	-2.820	2.301	0.000
CE-CZ-NU-CU	-4.184	-1.464	0.000	0.000
CE-OE-CE-CE	2.720	-1.046	2.803	0.000
CE-OE-CE-CZ	2.720	-1.046	2.803	0.000
CU-CB-CA-CB	0.000	30.334	0.000	0.000
CU-CB-CA-HC	0.000	30.334	0.000	0.000
CU-NU-CZ-HZ	0.000	0.000	0.741	0.000
CZ-CZ-NU-CU	-4.184	-1.464	0.000	0.000
CZ-NU-CU-CB	0.000	836.800	0.000	0.000
HE-CE-CE-HE	0.000	0.000	1.255	0.000
HE-CE-CE-OE	0.000	0.000	1.958	0.000
HE-CE-CZ-CZ	0.000	0.000	1.255	0.000
HE-CE-CZ-HZ	0.000	0.000	1.255	0.000
HE-CE-CZ-NU	0.000	0.000	-2.435	0.000
HE-CE-OE-CE	0.000	0.000	3.180	0.000
HU-CU-NU-CZ	0.000	41.840	0.000	0.000
HZ-CZ-CZ-HZ	0.000	0.000	1.255	0.000
NU-CU-CB-CA	0.000	30.334	0.000	0.000
NU-CZ-CZ-HZ	0.000	0.000	-2.435	0.000
NU-CZ-CZ-NU	46.170	-4.050	1.130	0.000
OE-CE-CE-OE	-2.301	0.000	0.000	0.000
OE-CE-CZ-CZ	7.159	-2.092	2.774	0.000
OE-CE-CZ-HZ	0.000	0.000	1.958	0.000
OE-CE-CZ-NU	33.472	0.000	0.000	0.000

Supplementary Table S8. Atom type parameters for methane

Atom Type	Mass	Charge [e]	σ [nm]	ε [kJ mol^{-1}]
CT	12.0110	-0.2400	0.3500	0.2761
HH	1.0800	0.0600	0.2500	0.1255

Supplementary Table S9. Bond stretching parameters for methane

Bond Type	k_r [kJ mol^{-1} nm^{-2}]	r_{eq} [nm]
CT-HH	284512.0000	0.1090

Supplementary Table S10. Bond bending parameters for methane

Angle Type	k_θ [kJ mol^{-1} rad^{-1}]	θ_{eq} [^{o}]
HH-CT-HH	276.1440	107.8000

4. Positron annihilation lifetime spectroscopy (PALS) experiments

4.1. Experimental procedure

Experiments were performed in a device that was described previously.[14-16] Special care was taken to ensure consistency between measurements, and we therefore used the same Na-22 source encapsulated in Kapton, the same counting rate of *ca.* 250 cts/s (total counts 5×10^6), the same temperature program (accuracy ±1 K), and the same evaluation method and boundary conditions throughout. Unless otherwise stated measurements were done in the standard configuration with sample material placed into one Al pan covered with Kapton foil. Measurements on the porous liquid at room temperature were made with an alternative sample holder shown in **Supplementary Figure S20** in which the radioactive source is surrounded by two samples of the material.

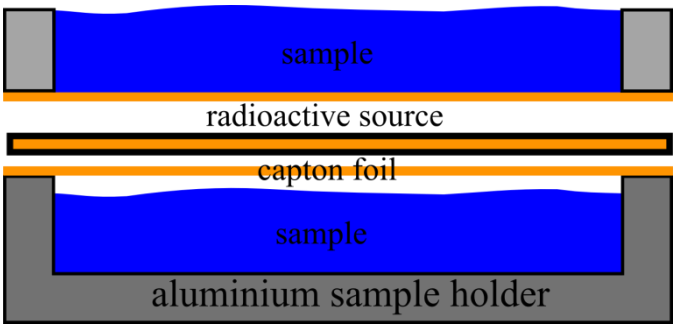

Supplementary Figure S20 PALS measurement set-up for the porous liquid sample.

This sandwich-like arrangement enhances the o-Ps intensity because more positrons can annihilate in the material. All spectra were evaluated with the software LT 9.2 with a free fit for all parameters,[17] unless stated otherwise. First, all three materials, the pure crown ether, the pure solid cage, and the porous liquid, were measured independently as a function of temperature. The data are shown in **Supplementary Figure S21**. For the following figures, the o-Ps lifetime is shown the upper part and labeled (a), the corresponding o-Ps intensity data in the lower part, labeled (b).

(a)

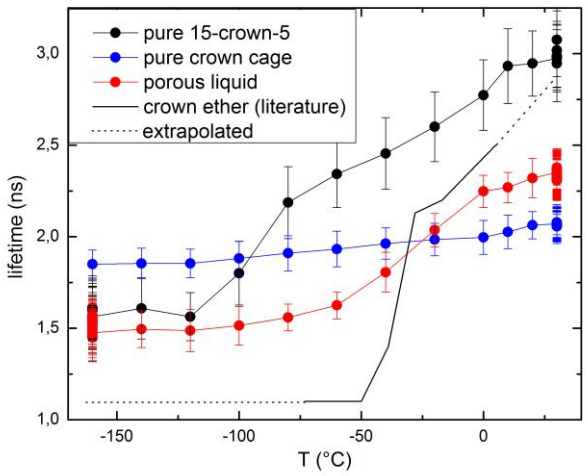

(b)

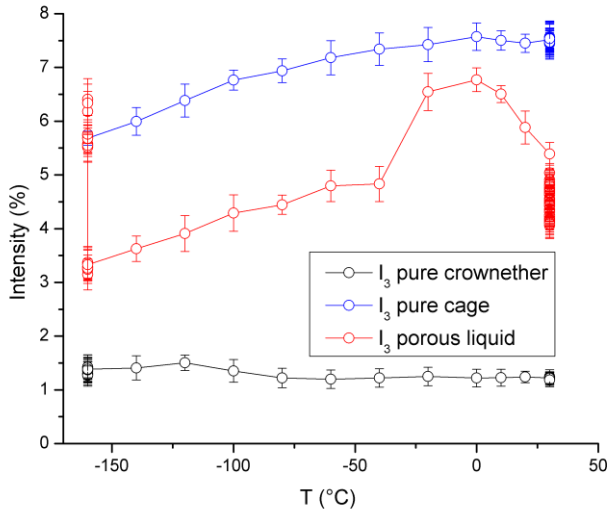

Supplementary Figure S21 (a) Plot of o-Ps lifetime (τ_3) as function of temperature for all samples. Literature data (Mahmood et al., ref. 18, for details see text) are also included and extrapolated to higher temperature for comparison with our data (b) corresponding o-Ps intensities. Note that repeated measurements were performed at –160 °C and at + 30 °C to enable clear separation of the respective contributions of the cage and the 15-crown-5 solvent.

Supplementary Figure S21 shows the o-Ps lifetimes and intensity data for the porous liquid, the pure solid cage and the pure 15-crown-5, together with o-Ps lifetime data for 15-crown-5 taken from the literature.[18] Regarding lifetimes, the temperature dependencies of the o-Ps lifetimes, τ_3, are different for each of the three materials. At room temperature, the lifetime measured for the porous liquid lies between that of the pure crown-ether solvent and the pure cage. Hence, a clear differentiation of the contributions made by the crown-ether solvent and the dissolved cages in the porous liquid is not straightforward. Regarding intensities, the o-Ps intensity is a product of o-Ps formation and hole concentration, and the former contribution is usually not known. Also, in composite materials such as the porous liquid analysed here, preferential trapping in one constituent can occur. Thus, a direct obvious interpretation of the observed o-Ps intensities is not appropriate based only on these data.

4.2. Comparison with literature data for 15-crown-5

The spectra for the porous liquid are a (potentially nonlinear) superposition of the spectra of pure cage and pure 15-crown-5. These contributions might not be straightforward to separate in the PALS spectra. Thus we also investigated pure solid cage and pure 15-crown-5 samples. The latter was not straightforward, as the equipment used here is not perfectly suited for low viscosity liquids due to the risk of leakage (see sample holder, **Supplementary Figure S20**). Hence the amount of material we could analyse for 15-crown-5 using just one pan was relatively small and the respective intensities we observed were lower than for the literature on previous measurements on 15-crown-5.[18] Comparing our data for 15-crown-5 (**Supplementary Figure S21**, black dots) with the literature data for 15-crown-5 the agreement at higher temperatures is good, if we extrapolate the literature data up to +30 ^{o}C. However, at low temperature we measure approximately 1.6 ns whereas the literature value is approximately 1 ns. For completeness, we include our low temperature data in the following fitting analysis. However, because of the discrepancy between our low temperature data and the literature data for 15-crown-5, we refrain from drawing conclusions from the low temperature data and base our conclusions only on the room temperature data.

4.3. Data Analysis

In order to separate the o-Ps lifetimes of the empty cage and the pure crown ether, we made several measurements with the porous liquid at both −160 ºC and at +30 °C. This allowed us to check for measurement reproducibility and to provide a clear separation of the two contributions (**Supplementary Figures S22** and **S23**). Here, some clarification in the definition of variables is necessary. By convention, the o-Ps lifetime is termed τ_3. If we split this into two components, we term these τ_{3A} and τ_{3B}, with τ_{3A} being the shorter and τ_{3B} the longer of the two components. The strong temperature dependence of the o-Ps lifetime for 15-crown-5 leads to the cross-over of traces as can be seen in **Supplementary Figure S21**. Note that because of this, the assignment of τ_{3A} or τ_{3B} to the lifetime of a particular component (cage or 15-crown-5 solvent) in the porous liquid changes with temperature. At - 160 °C, τ_{3A} is attributed to the 15-crown-5 solvent component of the porous liquid (and correspondingly τ_{3B} to the cage component), whereas at + 30 °C τ_{3A} is attributed to the cage component (and accordingly τ_{3B} to the crown ether).

To separate the o-Ps lifetime measured for the porous liquid into its components, we used two general approaches, specifically free fits and forced fits. In the free fits no constraints were applied to the o-Ps lifetime components (**Supplementary Figures S22** and **S23**). For the forced fits, one of the o-Ps lifetime components was constrained to 3.00 ns to correspond to the 15-crown-5 component.

(a)

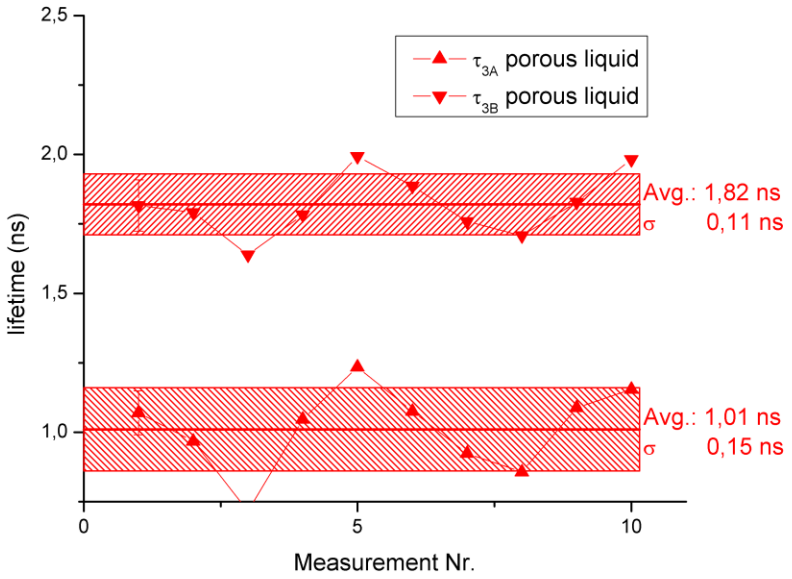

(b)

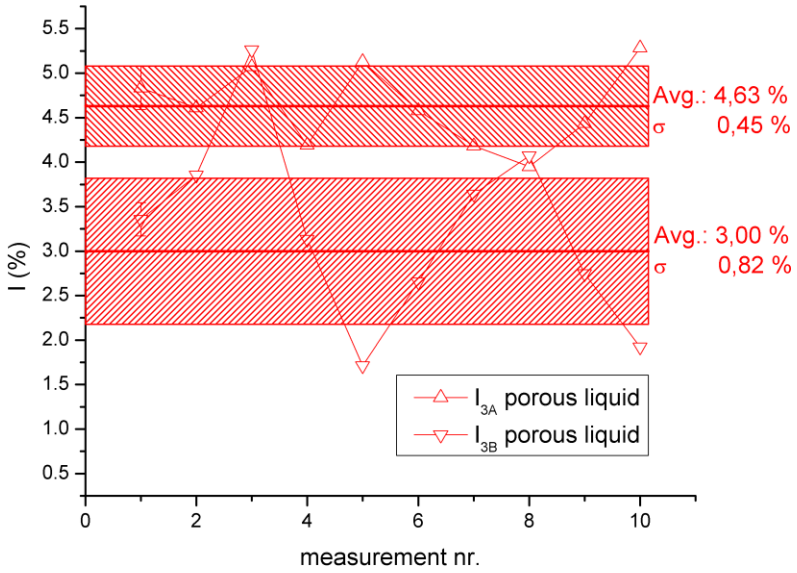

Supplementary Figure S22 (a) Components of the lifetime, τ_{3A} & τ_{3B}, for the porous liquid at –160 °C (free fit). For the first data point the error bar for the individual measurement is attached. The dashed rectangles indicate mean values and standard deviations, respectively. (b) Components of the o-Ps intensity for the porous liquid at –160 °C. The error bar is illustrated measurement number 1. The horizontal red lines and dashed rectangles indicate mean values and standard deviations, respectively.

(a)

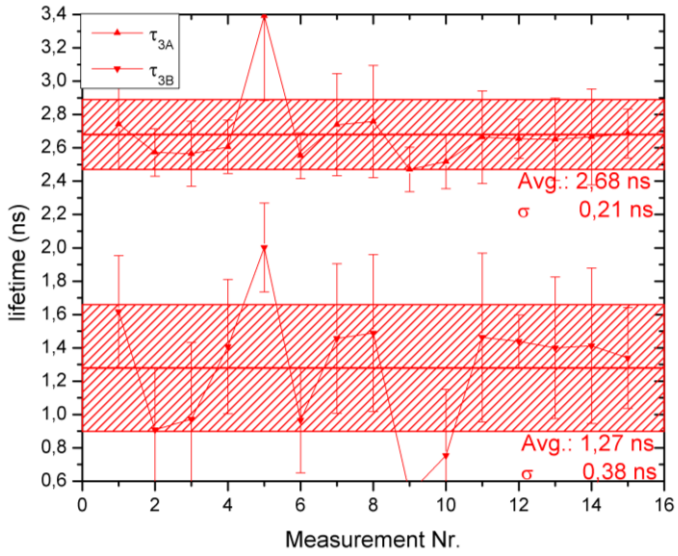

(b)

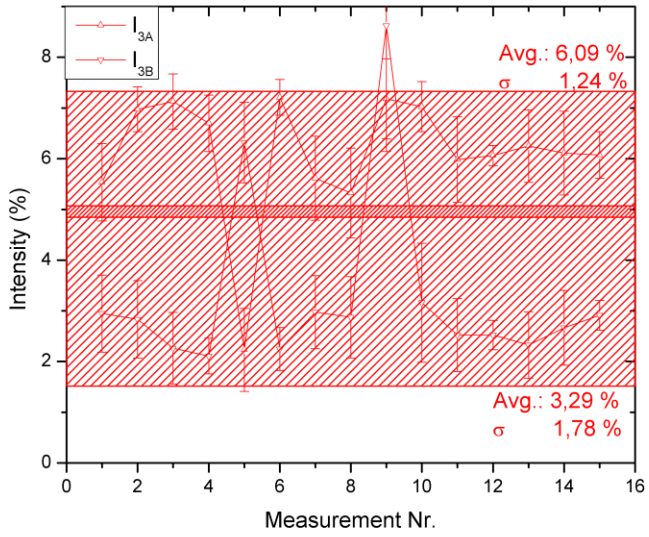

Supplementary Figure S23 (a) Components of the lifetime, τ_{3A} & τ_{3B}, for the porous liquid at + 30 °C (free fit). The horizontal red lines and dashed rectangles indicate mean values and standard deviations, respectively. (b) Components of the o-Ps intensity for the porous liquid at + 30 °C. The dashed rectangles indicate standard deviations.

Supplementary Figure S22, where all parameters were freely fitted, shows the separation of the observed lifetime, τ_3, into two contributions, denoted τ_{3A} and τ_{3B}, for the porous liquid sample at –160 °C. The values of τ_{3A} and τ_{3B} coincide with the expected values for empty cage and with the literature value[18] of the crown ether. However, as noted above, due to the discrepancy between our low temperature measurements on the pure 15-crown-5 and those in the literature, we refrain from making any conclusions regarding the significance of this fitting.

Supplementary Figure S23 shows the separation of τ_3 into the two contributions, τ_{3A} and τ_{3B}, for the porous liquid sample at + 30 °C. Again, all parameters were freely fitted. The dashed rectangle shows the mean value with the respective standard derivation. The free fit reveals that there are two long lifetime components present. As a control, we also attempted the same procedure to fit two o-Ps lifetime components to the o-Ps lifetime data for the pure crown ether. However, in that case it was not possible to find two lifetime components. This is consistent with the absence of dissolved cages in the pure 15-crown-5.

The values of τ_{3A} and τ_{3B} obtained from the fitting in **Supplementary Figure S23** (a) are clearly different to those expected for two components based on the observed lifetimes for the pure cage and pure 15-crown-5 at + 30 ^{o}C and clearly also fluctuate strongly. Therefore, we performed a forced fit (**Supplementary Figure S24**) in which τ_{3B} was fixed at 3.00 ns, the value obtained for the pure 15-crown-5. This improved the apparent error, reduced the fluctuation in the data, and provided a value of τ_{3A} of 1.91 ns which corresponds well to the value obtained for the pure solid cage of 2.05 ns +/- 0.1 ns.

Key o-Ps lifetimes are summarized in **Supplementary Table S11**.

(a)

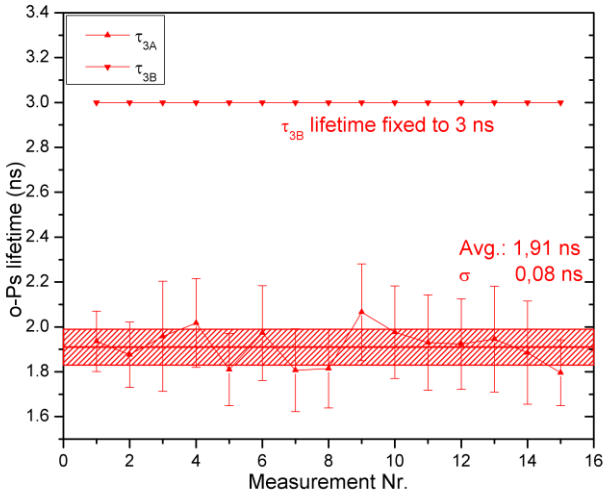

(b)

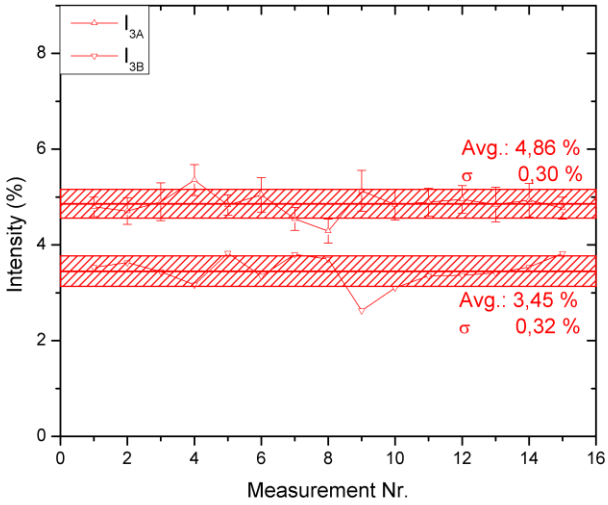

Supplementary Figure S24 (a) Components of the lifetime, τ_{3A} & τ_{3B}, for the porous liquid at + 30 °C (τ_{3B} fixed at 3.00 ns, τ_{3A} free). The horizontal red lines and dashed rectangles indicate mean values and standard deviations, respectively. (b) Components of the o-Ps intensity for the porous liquid at 30 °C. I_{3A}: intensity corresponding to τ_{3A}; I_{3B}: intensity corresponding to τ_{3B}. The horizontal red lines and dashed rectangles indicate mean values and standard deviations, respectively. Please note that the o-Ps intensities are not fixed.

Supplementary Table S11 PALS o-Ps lifetime results for the pure 15-crown-5, the pure crown cage and the porous liquid.*

Sample	o-Ps lifetimes (ns) observed or fitted at -160 °C	o-Ps lifetimes (ns) observed or fitted at + 30 °C	Interpretation
pure 15-crown-5	1.60 +/- 0.1	3.00 +/- 0.1	T= - 160 °C: o-Ps lifetime inside the crown ether ring.** T = + 30 °C; o-Ps bubble lifetime of 15-crown-5
pure cage	1.85 +/- 0.1	2.05 +/- 0.1	Lifetime inside the cages
porous liquid	*Observed value:* 1.52 +/- 0.04	*Observed value:* 2.34 +/- 0.02	Separation of o-Ps lifetime into two components corresponding to 15-crown-5 solvent and empty dissolved cages is satisfactory for +30 °C data when one component (τ_{3B}) is fixed (forced fit).
	Free fit: 1.82 +/- 0.11, 1.01 +/- 0.15	*Free fit:* 2.68 +/- 0.21, 1.27 +/- 0.38	
	-	*Forced fit:* 3.00 (fixed) 1.91 +/- 0.08	

*** Error bars given here are standard deviations of the average of several measurements (typically 15) at constant temperature. Standard errors would correspondingly be lower by a factor of 0.25.**

**** for a discussion of the discrepancy between the literature value[18] and our data at -160 °C see section "4.2 Comparison with literature data for 15-crown-5" above.**

5. Measurement of gas solubilities in the crown-cage porous liquid

An isochoric technique[19] was used to measure methane gas solubility in the pure 15-crown-5 and in the porous liquid. In this technique, a known quantity of gaseous solute is placed in contact with a gravimetrically determined quantity of degassed solvent at a constant temperature inside an accurately known volume. When thermodynamic equilibrium is attained at a given temperature, the pressure above the liquid solution is constant and is directly related to the quantity of gas absorbed by the liquid.

A schematic drawing of the glass apparatus used is represented in **Supplementary Figure 25**. The equilibrium cell EC, together with the precision manometer M and the glass bulb limited by valve V2, constitute the equilibrium section of the apparatus. The simple design of the equilibrium cell is appropriate for the study of viscous liquids like the porous liquid measured here. The equilibrium cell permits to handle volumes of liquid solvent varying from (0.5 to 3) mL and normally an appropriate gas/liquid contact is guaranteed by means of good agitation using a glass coated magnetic bar. In the case of the porous liquid, a small quantity of solvent was used, it formed a thin film on the walls of the equilibrium cell and for this reason, it was not necessary to use the stirrer bar to insure a good gas-liquid contact. The whole equilibrium section was maintained inside a 500 L water bath (TB in **Supplementary Figure 17**) at constant temperature to within ±0.01 K using a PID temperature controller and accurately measured with a calibrated 100 Ω platinum resistance thermometer from Hart Scientific (Secondary Reference Temperature Standard, model 5612, accuracy of ±0.018 °C at 0 °C).

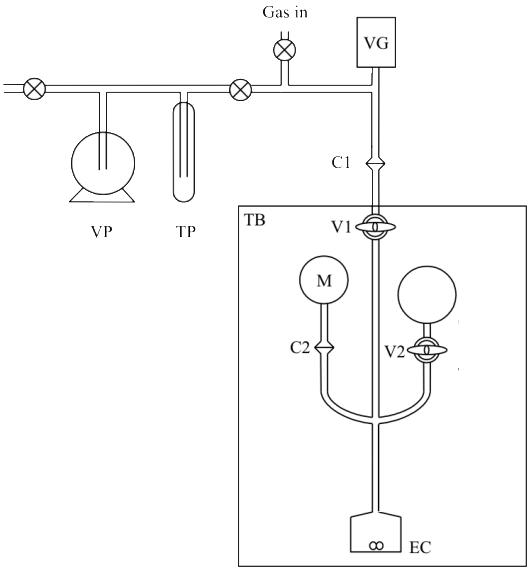

Supplementary Figure 25. Schematic drawing of the gas absorption apparatus used in this work. VP vacuum pump; TP, cold trap; VG, vacuum gauge; M, precision manometer; TB, thermostated liquid bath; EC, equilibrium cell; V1, V2, constant volume glass valves; C1, C2, vacuum O'ring connections.

The gas absorption determination starts by the introduction of a known quantity of methane in the calibrated glass bulb limited by valve V2. The exact amount of gas is determined by measuring its pressure in the manometer M (Druck RPT 2005, (15 to 1800) mbar, precision of 0.01% full scale), at constant temperature, correcting for gas imperfection. The volume of the gas bulb, $V_2 = (55.14 \pm 0.02)$ cm^3 at 303 K, was previously calibrated by weighting it full of a liquid of known density with a precision better than ± 0.01%. The volume was determined at two different temperatures in order to correctly account for the thermal expansion corrections (volumetric thermal expansion coefficient $\alpha = 2.76 \times 10^{-5}$). Once the pressure and temperature are stable (thus allowing the determination of the quantity of the gas contained in bulb V2), the glass valve V2 is closed.

A gravimetrically determined quantity of liquid solvent (with a precision of 1×10^{-4} g), equal to 2.6535 g for the pure 15-crown-5 ether and 1.0127 g for the porous liquid[20], was in each case introduced in the equilibrium cell through connection C2. The liquid solvent is degassed by keeping it under a primary vacuum (approximately 1 Pa) for several hours.

The gas-liquid equilibrium process starts by closing valve V1 and bringing into contact the gas and the liquid solvent thru opening valve V2. The total volume of the measuring cell delimited by valve V1, V_{tot} = (80.14 ± 0.06) cm^3 at 303.26 K, was previously calibrated by gas expansions from the gas bulb, at different temperatures in order to take into account the thermal expansion corrections (volumetric thermal expansion coefficient $\alpha = 8.67 \times 10^{-5}$). The pressure and temperature during the methane/liquid solvent equilibration processes were recorded in a computer until a constant temperature (to within ± 0.01°C) and a constant pressure (to within ± 0.05 mbar) were attained. The vapour pressure of both the pure 15-crown-5 ether and of the porous liquid is sufficiently low to be ignored, in the temperature range studied, without introducing a significant uncertainty (< 15 mbar, the lower pressure read by the manometer used).

The determination of methane absorption by the 15-crown-5 ether and by the porous liquid at different temperatures was done by changing the liquid thermostat set point and waiting for a new thermodynamic equilibrium at a different temperature. With a single loading it is thus possible to make measurements as a function of temperature. For the 15-crown-5 ether, several runs were performed using fresh liquid and gas samples. For the porous liquid, only one sample was used to determine the methane absorption as a function of temperature.

5.1. Gas absorption results

For each gas absorption experiment, the equilibrium temperature and pressure were used to calculate the mole fraction solubilities of methane in the pure 15-crown-5 ether and in the solution of porous liquid. The mole fraction gas solubility, x_{gas}, is defined as the maximum amount of gas absorbed by the liquid at a given temperature and pressure:

$$x_{gas} = \frac{n_{gas}}{\left(n_{gas} + n_{liq}\right)}$$

where n_{gas} is the amount of methane absorbed by n_{liq} moles of liquid solvent. The quantity of solvent is determined gravimetrically and the amount of methane is is calculated by the difference between two *pVT* measurements: first when the gas is introduced in the calibrated bulb with volume V_2 and second after thermodynamic equilibrium is reached:

$$n_{liq} = \left[\frac{p_{\text{ini}} V_2}{Z_{CH_4}\left(p_{\text{ini}}, T_{\text{ini}}\right) R T_{\text{ini}}}\right] - \left[\frac{p_{\text{eq}}\left(V_{\text{tot}} - V_{\text{liq}}\right)}{Z_{CH_4}\left(p_{\text{eq}}, T_{\text{eq}}\right) R T_{\text{eq}}}\right]$$

where p_{ini} and T_{ini} are the pressure and temperature in the first *pVT* determination and p_{eq} and T_{eq} the pressure and temperature at the equilibrium. V_{tot} is the total volume of the equilibration cell, Vliq is the volume of the liquid solvent[20] and Z_{CH4} is the compression factor for the pure gas.

The values of the mole fraction gas absorption measured at the different temperatures (listed in the fourth columns of **Supplementary Tables 12–14**) are difficult to compare because the equilibrium pressure is different for each gas absorption experiment, as listed in the second column these tables. In order to compare the different measured gas solubilities, Henry's law constants were calculated from the experimental values, assuming the vapour pressure of both the pure 15-crown-5 ether and of the porous liquid is sufficiently low to be ignored:

$$K_{\text{H}} = \lim_{x_{CH4} \to 0} \frac{f_{CH_4}\left(p, T, x_{CH_4}\right)}{x_{CH_4}} \cong \frac{\phi_{CH_4}\left(p_{\text{eq}}, T_{\text{eq}}\right) p_{\text{eq}}}{x_{CH_4}}$$

where f_{CH4} is the fugacity of the solute and ϕ_{CH4} its fugacity coefficient. These values of K_H were then used to determine the methane absorption at each temperature, assuming a partial pressure of methane equal to 1 bar:

$$x_{CH_4} = \frac{\phi_{CH_4}\left(p = 1\,bar, T\right)}{K_H}$$

The different values for the gas absorption are then comparable, as reported in the right-hand columns of **Supplementary Tables 12–14** at the same partial pressure of solute above the liquid. The non-ideality of the gas was taken into account at the level of the second virial coefficient[21]. The overall uncertainty of the mole fraction solubility reported is **Supplementary Tables 12** and **13** is estimated as ± 5%[22].

Supplementary Table 12 Methane solubility in pure 15-crown-5 ether solvent.

t /°C	p/mbar	$n^{⌘}_{liq}$/mol	$n_{gas\ diss}$ /mol	Solubility*		
				x_{gas}	n_{gas}/n_{liq}	$(n_{gas}/m_{liq})/\mu molg^{-1}$
30.09	625.60	1.20×10^{-2}	1.11×10^{-5}	1.5×10^{-3}	1.5×10^{-3}	6.7
40.09	646.22	1.20×10^{-2}	0.93×10^{-5}	1.2×10^{-3}	1.2×10^{-3}	5.4
50.10	666.89	1.20×10^{-2}	0.73×10^{-5}	0.9×10^{-3}	0.9×10^{-3}	4.1
60.08	687.87	1.20×10^{-2}	0.42×10^{-5}	0.5×10^{-3}	0.5×10^{-3}	2.3

* Values calculated for a 1 bar partial pressure of gas
⌘ Corresponding to 2.6535 g of 15-crown-5 ether (molecular weight = 220.27 $g{\cdot}mol^{-1}$)

Supplementary Table 13 gives the methane solubility in the porous liquid, which is a 1:12 molar ratio solution of the crown cage in the 15-crown-5 solvent. The molecular weights of the crown cage and of the 15-crown-5 ether solvent are 2102.45 $g{\cdot}mol^{-1}$ and 220.27 $g{\cdot}mol^{-1}$, respectively.

Supplementary Table 13 Methane solubility in the porous liquid; this is a 1:12 molar (or 8.3 % mol/mol) solution of crown cage dissolved in 15-crown-5 ether.

t /°C	p/mbar	$n^{⌘}_{sol}$/mol	$n_{gas\ diss}$ /mol	Solubility*		
				x_{gas}	n_{gas}/n_{sol}	(n_{gas}/m_{sol})/μmol g^{-1}
30.10	616.09	2.69×10^{-3}	3.23×10^{-5}	1.9×10^{-2}	0.020	52
40.11	636.29	2.69×10^{-3}	3.09×10^{-5}	1.7×10^{-2}	0.018	48
50.68	659.44	2.69×10^{-3}	2.35×10^{-5}	1.3×10^{-2}	0.013	35

* Values calculated for a 1 bar partial pressure of gas
⌘ Corresponding to 1.0127 g of porous liquid. The molecular weight of the porous liquid solution is calculated as $MW_{sol} = x_1 MW_1 + x_2 MW_2 = 365.05\ g \times mol^{-1}$, x_1 and x_2 being the mole fractions of crown cage and of 15-crown-5 ether in the porous liquid with molecular weights MW_1 and MW_2, respectively.

Supplementary Table 14 reports the methane solubility considering only the crown cage component in the porous liquid. If the uncertainty on the preparation and handling of the solution of crown cage in the 15-crown-5 is taken into account, a maximum overall uncertainty of the mole fraction solubility reported is Supplementary Table 14 is estimated as ± 10%

Supplementary Table 14 Methane solubility in the crown cage, calculated using the values in **Supplementary Table 13**)

t /°C	p/mbar	n_{cage}/mol	$n_{gas\ diss}$ /mol	Solubility*		
				x_{gas}	n_{gas}/n_{cage}	(n_{gas}/m_{cage})/ μmolg^{-1}
30.10	616.09	2.23×10^{-4}	3.23×10^{-5}	0.20	0.25	119
40.11	636.29	2.23×10^{-4}	3.09×10^{-5}	0.19	0.23	109
50.68	659.44	2.23×10^{-4}	2.35×10^{-5}	0.14	0.17	77.8

* Values calculated for a 1 bar partial pressure of gas

6. Scrambled cages: synthesis, characterization, gas solubilities, and guest selectivities

6.1. One-pot synthesis of scrambled cages

The scrambled cage mixture was prepared in one step according to the following scheme:

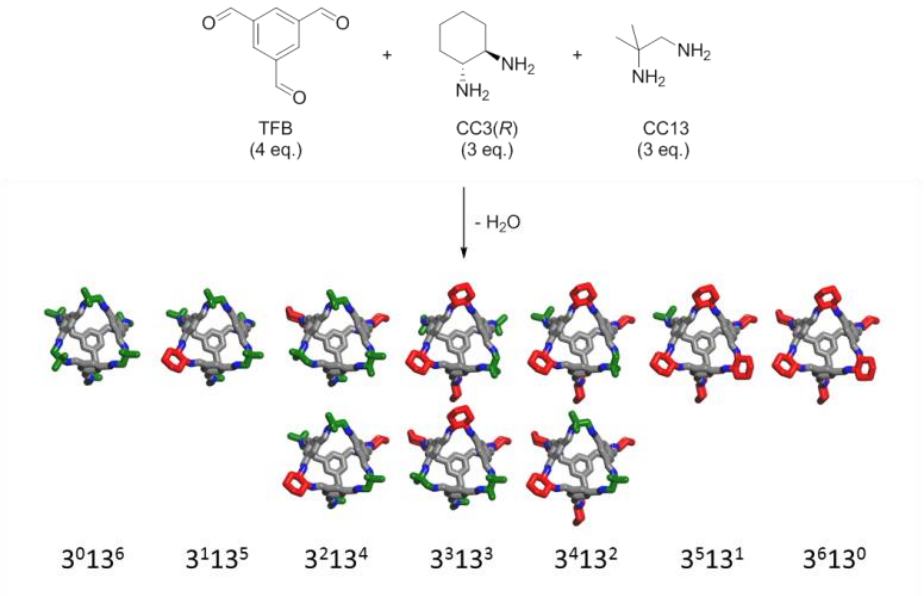

To a 3 L jacketed vessel, equipped with overhead stirrer, was added 1,3,5-triformylbenzene (7.5 g, 46.25 mmol, 4 eq.) in DCM (2.25 L), followed by solutions of (*R*,*R*)-1,2-diaminocyclohexane[23] (3.961 g, 34.69 mmol, 3 eq.) in DCM (225 mL) and 1,2-diamino-2-methylpropane[24] (3.058 g) in DCM (225 mL). The resulting solution was stirred at 20 °C under N_2 for 3 days and the reaction completion checked by HPLC analysis before concentration *in vacuo*. The crude product was redissolved in DCM (250 mL) and filtered to remove any insoluble solids before concentration *in vacuo*. The resulting yellow solid was washed with EtOAc (3 × 50 mL) and the collected solid completely dissolved in DCM before concentration *in vacuo* prior to drying in the vacuum oven at 90 °C overnight to afford a very pale yellow solid (9.33 g, 77%).

IR (ν_{max} /cm^{-1}) 2927, 2856, 1648 (imine, N=C), 1598, 1444, 1380, 1365, 1147, 1093, 1054; **^{1}H NMR** (400 MHz, $CDCl_3$) δ_H 8.22-7.78 (24H, m, N=C*H* and Ar*H*), 3.95-3.35 (12H, m, C*H*N=CH), 1.84-1.31 (42H, m, CH_2 and CH_3); **^{13}C NMR** (101 MHz, $CDCl_3$) δ_C (*NB.* Due to scrambling all

^{13}C NMR signals are broad mulitplets) 160.9, 159.2, 155.3, 137.1, 136.6, 129.4, 74.8, 72.3, 61.2, 33.1, 29.5, 24.4, 22.2; **MS** (TOF ES+) calc. for scrambled cages 3^0:13^6, 3^1:13^5, 3^2:13^4, 3^3:13^3, 3^4:13^2, 3^5:13^1, 3^6:13^0 = 960.6, 986.6, 1012.6, 1038.66, 1064.68, 1090.7, 1116.7; found $[M+H]^+$ 961.6, 987.6, 1013.6, 1039.7, 1065.7, 1091.7, 1119.7.

The various possible compositions in the scrambled cages can be denoted according to the formula $\mathbf{3^{6-n}13^n}$, where *x* represents the number of diaminocyclohexane vertices in the cage, and *n* represents number 1,2-diamino-2-methylpropane vertices.[25] The scheme above illustrates the 10 possible permutations: for $\mathbf{3^2 13^4}$, $\mathbf{3^3 13^3}$ and $\mathbf{3^4 13^2}$, there are two possible isomers for each combination.

6.2. NMR spectra of $3^{6-n}13^{n}$ scrambled cage mixture

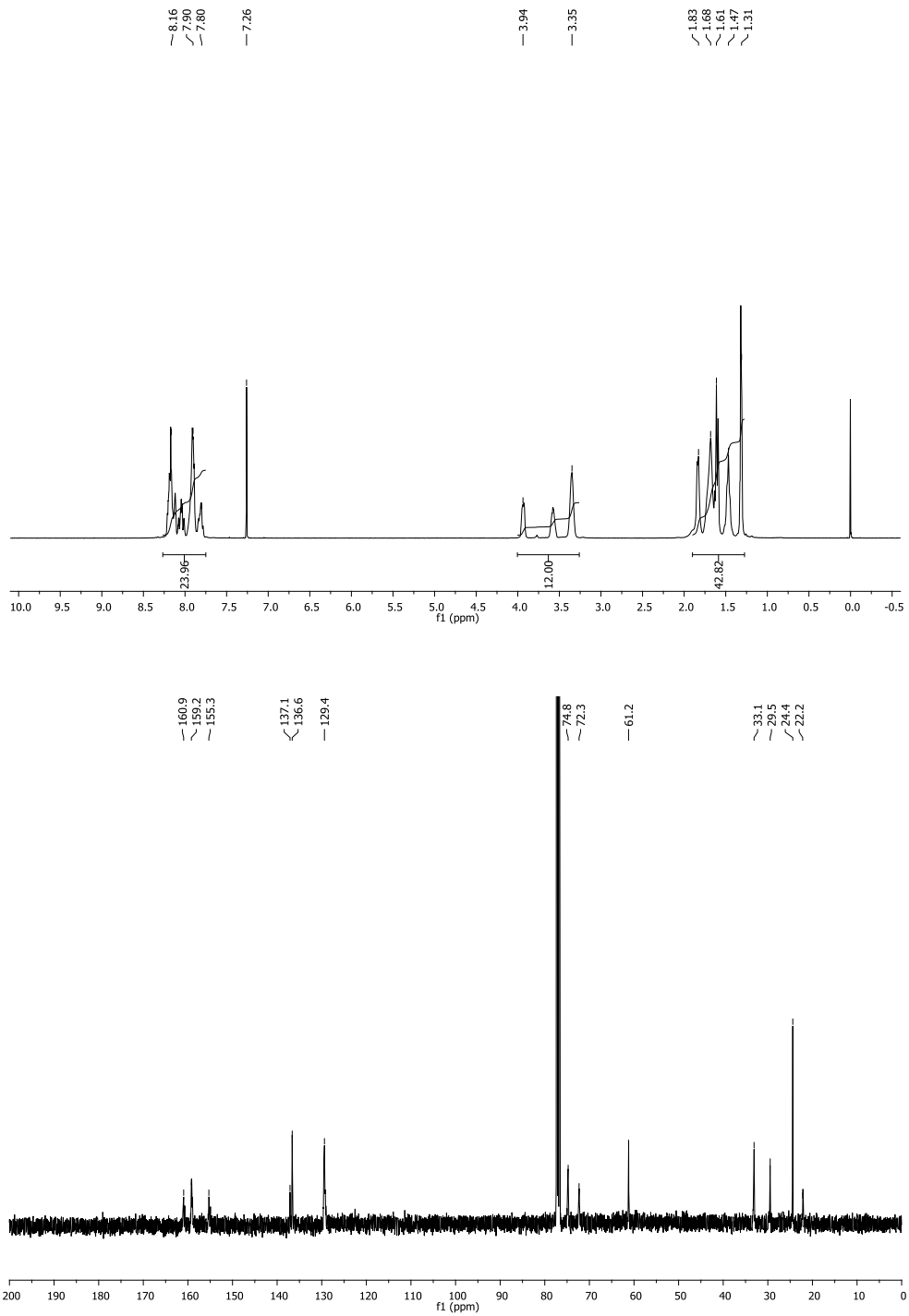

Supplementary Figure 26. ^{1}H NMR ($CDCl_3$; upper) and ^{13}C NMR ($CDCl_3$; lower) for the $\mathbf{3^{6-n}13^{n}}$ scrambled cage mixture.

6.3. HPLC analysis for $3^{6-n}13^n$ scrambled cage mixture

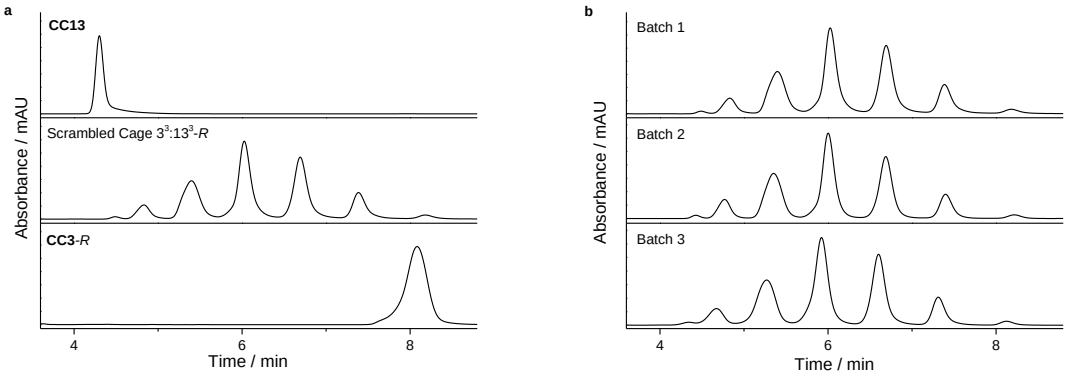

Batch	Peak Area / %						
	$3^0 13^6$	$3^1 13^5$	$3^2 13^4$	$3^3 13^3$	$3^4 13^2$	$3^5 13^1$	$3^6 13^0$
1	0.61	6.67	21.50	33.11	26.32	10.36	1.43
2	0.86	7.21	22.76	33.08	24.98	9.71	1.39
3	0.35	5.55	21.98	34.54	26.71	9.44	1.42

Supplementary Figure 27. HPLC analysis for $3^{6-n}13^n$ scrambled cages. **a,** Comparison of HPLC data for the parent cages, **CC3**-*R* (bottom) and **CC13** (top), which contain just one diamine in each cage,[23,24] with the scrambled $\mathbf{3^3{:}13^3}$-***R*** cage mixture (middle). Note that the two possible isomers for each of the $\mathbf{3^2 13^4}$, $\mathbf{3^3 13^3}$ and $\mathbf{3^4 13^2}$ compositions are not resolved under these analysis conditions, hence we see only 7 peaks, not 10 (see scheme in **6.1**). (b) Overlay of HPLC traces for three different batches of the $\mathbf{3^3{:}13^3}$-***R*** scrambled cages; the table below shows the corresponding peak areas for each cage component. The batches are relatively reproducible, with the $\mathbf{3^2 13^4}$, $\mathbf{3^3 13^3}$ and $\mathbf{3^4 13^2}$ cages (in likelihood 6 different species, including isomers) making up around 80 mol. % of the total mixture.

6.4. Thermogravimetric analysis of the $3^{6-n}13^{n}$ scrambled cage mixture and the porous liquid

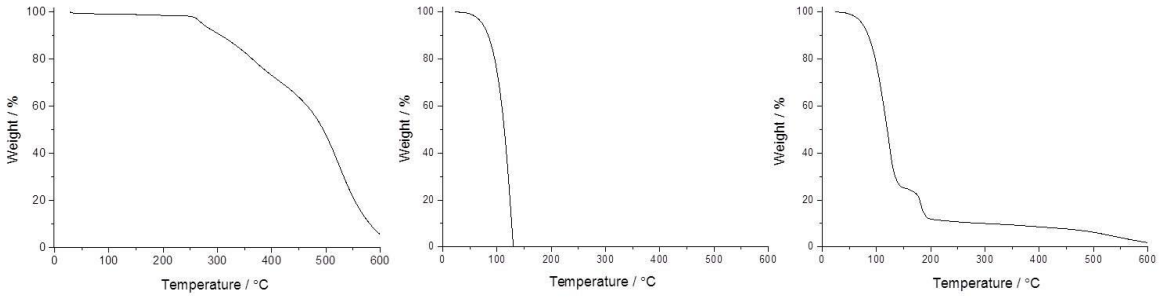

Supplementary Figure 28. TGA was conducted at a ramp rate of 5 °C/min up to 600 °C in an aluminium pan under a nitrogen flow for **a)** the scrambled $\mathbf{3^{6-n}13^{n}}$ cage referred to in **6.1**; **b)** hexachloropropene, and; **c)** the porous liquid (1:36 cage:hexachloropropene).

6.5. Purification of hexachloropropene solvent

We found that different batches of hexachloropropene often had markedly different impurity profiles. The solvent was therefore rigourously purified before use. This is important because the properties of the porous liquid might be strongly affected by even trace impurities in the solvent, such as other chlorinated molecules that are small enough to occupy the cage cavities.

Hexachloropropene (~510 mL, 9 × 100 g bottles, Sigma-Aldrich, H6401, batch MKBQ2222V) was filtered 5 times through 5 separate activated basic alumina plugs (5 × 150 g aluminium oxide, activated, basic, Brockmann I, CAS 1344-28-1, Sigma-Aldrich) using positive N_2 pressure to afford pure hexachloropropene (175 mL, 34 % recovery); **^{13}C NMR** (126 MHz, d_2-DCM/TMS capillary) δ_C 132.1, 127.2, 92.8.

The purified hexachloropropene was transferred to a dry Schlenk tube and degassed *via* repeated freeze-pump-thaw cycles before being stored under N_2 and used for the porous liquid studies. All experiments used this purified solvent (**Supplementary Figures 29 & 30**).

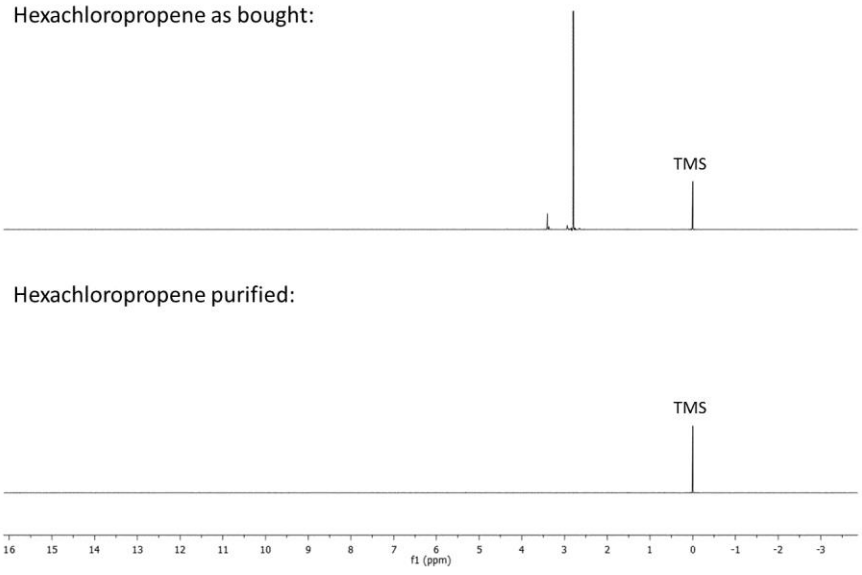

Supplementary Figure 29. ^{1}H NMR (d_2-DCM/TMS capillary) spectra of hexachloropropene – before and after purification through basic alumina.

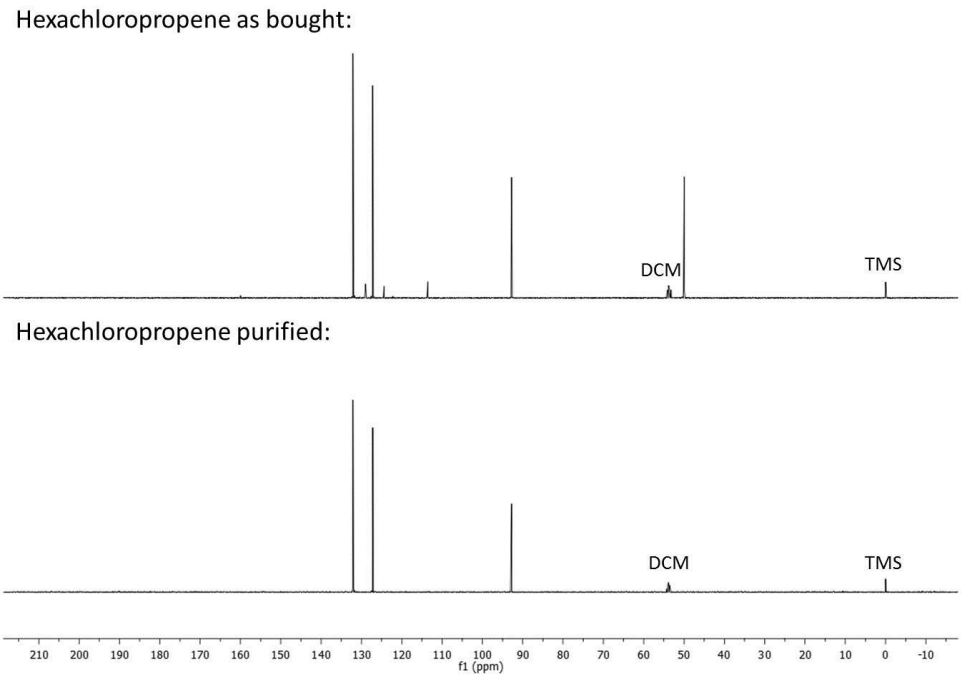

Supplementary Figure 30. ^{13}C NMR (d_2-DCM/TMS capillary) spectra of hexachloropropene – before and after purification through basic alumina

6.6. Purification of 1-*t*-butyl-3,5-dimethylbenzene solvent

A second 'bulky' solvent, 1-*t*-butyl-3,5-dimethylbenzene, was also examined and was rigorously purified for the same reasons (**6.6**). The solvent was purified by vacuum distillation with the first 10 % discarded; pure 1-*t*-butyl-3,5-dimethylbenzene was collected at 55 °C / 1.7 mbar.

6.7. Synthesis of the 'scrambled' porous liquid

The amorphous scrambled cage solid ***(R)*-3^{6-n}13^{n}** is porous (SA_{BET} = 520–640 m^2/g), so it was first desolvated / degassed in the solid state to remove any guests in the pores. The material was heated in a vacuum oven at 90 °C overnight before being evacuated and refilled with N_2 on a manifold, and subsequently dissolved in degassed hexachloropropene at a concentration of 20 % w_{cage}/v_{PCP} (*e.g.*, 200 mg dissolved in 1 mL PCP, 600 mg in 3 mL) to afford a pale yellow liquid. This concentration was chosen because it is just below the saturation solubility (234–242 mg/mL at RT).

Using the measured density of the purified hexachloropropene, the molar ratio of scrambled cage to solvent in the 20 % w/v porous liquid was calculated to be 1:35.8 (that is, around one cage for every 36 solvent molecules (average cage MW = 1039.34 g/mol; hexachloropropene MW = 248.75; density of pure hexachloropropene, ρ = 1.7127 g/mL).

6.8. NMR spectra of the 'scrambled' porous liquid in hexachloropropene

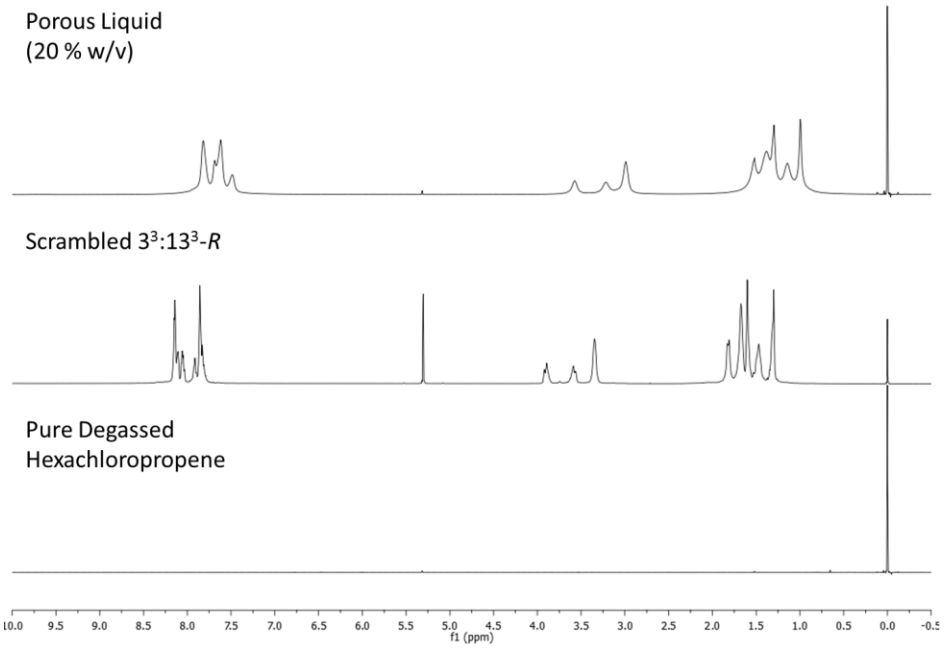

Supplementary Figure 31. Stacked ^{1}H NMR (d_2-DCM/TMS capillary) spectra of the porous liquid (top), the scrambled cage in d_2-DCM (middle) and hexachloropropene (bottom).

6.9. Methane solubility measurements in the 'scrambled' porous liquid by ^{1}H NMR

As for the crown cage (Fig. 3, main text), methane gas was found to be much more soluble in the scrambled cage porous liquid than in the neat, bulky solvent, PCP (**Supplementary Figure 32**). Confinement of the methane in the cages is also suggested by the strong shielding effect ($\Delta\delta$ = -2.56 ppm) for the methane ^{1}H NMR signal (**Supplementary Figure 32a,b**).

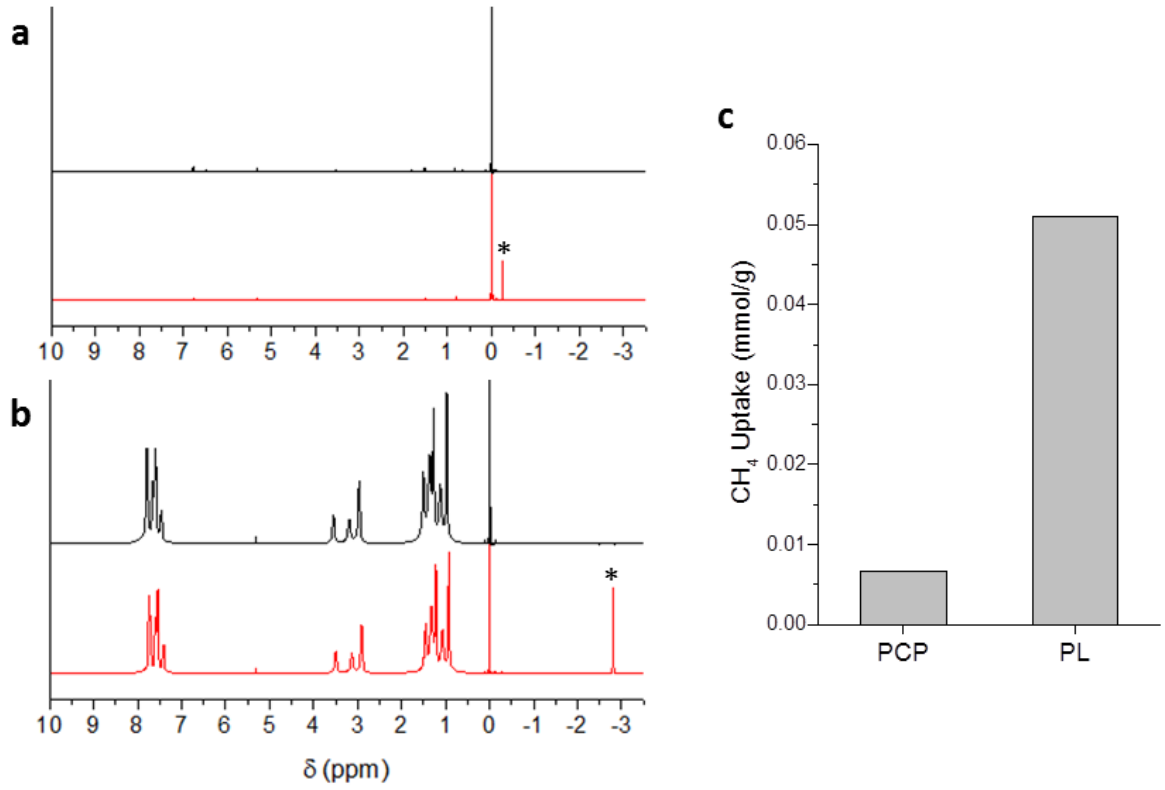

Supplementary Figure 32. Comparison of relative CH_4 uptake in the 'scrambled' porous liquid (PL) *vs* hexachloropropene (PCP) by ^{1}H NMR spectroscopy. a, Stacked ^{1}H NMR spectra for the neat PCP solvent both before (black) and after (red) CH_4 addition; CH_4 peak is labeled (*****) (**b**) Stacked ^{1}H NMR spectra for PL both before (black) and after CH_4 (red) addition with the CH_4 peak again labelled (*****) (**c**) Calculated CH_4 uptake for the PL and for PCP from the ^{1}H NMR spectra using a calibrated sealed capillary. A shift in the methane signal was observed, from -0.24 ppm in neat hexachloropropene to -2.80 ppm in the porous liquid.

6.10. Gas solubility measurements in the 'scrambled' porous liquid by volumetric gas evolution

The solubility of four different gases in the 'scrambled' porous liquid was also studied by volumetric gas evolution experiments, whereby solutions were saturated with gas prior to displacement of this gas by a guest molecule ($CHCl_3$).

Gas saturation: For the porous liquids, the scrambled cage (typically 600 mg, 0.5772 mmol) was added to a pre-weighed GC headspace vial (22 mm × 45 mm screw top, 10 mL, Fisher Scientific) equipped with a stirrer bar and lid. The lid was kept separate while the vial containing the scrambled cage solid was desolvated in a vacuum oven at 90 °C overnight. On removing the samples from the oven, the vials were immediately capped and reweighed to calculate the accurate quantity of desolvated / degassed scrambled cage present. The vial was connected to a manifold *via* a needle through the septum and evacuated for 10 min before N_2 was introduced prior to adding freeze-pump-thaw degassed hexachloropropene (typically 3 mL) to make up the 20 % w/v porous liquid. Once the cage was fully dissolved, the gas to be studied (N_2, CH_4, CO_2 or Xe) was then bubbled through the solution at a rate of 50–60 mL/min for 5 min per 1 mL of hexachloropropene (regulator output pressure set to 0.5 bar; gas flow was controlled with needle valve to achieve the desired flow rate, as measured using a calibrated Gilmont flowmeter scale with a stainless steel float). An 18 gauge needle was used as the gas outlet. For control experiments involving the solvent, hexachloropropene, the same procedure was employed: freeze-pump-thaw degassed hexachloropropene (typically 3 mL) was introduced without previous addition of the scrambled cage.

Gas evolution with 1:1 cage : $CHCl_3$ stoichiometry. The gas flow was stopped and the cap was rapidly changed for a new one with an unbroken septum. Using a syringe with a 21 gauge needle the gas being tested was used, whilst connected to the gas collection setup *via* a needle/tubing cannula, to set a start-point and ensure no air-locks remained. After marking the start-point, 1.0 eq. $CHCl_3$ (relative to the amount of cage present, typically 46 μL) was added. The sample was then stirred, allowing the $CHCl_3$ to fully mix with the porous liquid, and the gas evolution was measured by displacement of water in an inverted Rotaflo stopcock burette (10 or 25 mL with 0.1 mL graduations). These results are summarized in **Supplementary Figure 33**.

Attempted gas evolution with a bulky, size-excluded guest. These experiments were conducted on 20 % w/v porous liquid (600 mg cage dissolved in 3 mL hexachloropropene) saturated with gas according to the standard procedure above. For gas evolution, 1-*t*-butyl-3.5-dimethylbenzene (108 μL, 1.0 eq. based on cage) was used as the displacement solvent instead of $CHCl_3$. No gas was released upon addition of this bulky solvent. Subsequent addition of $CHCl_3$ (46 μL, 1.0 eq. based on cage) released the gas, as before.

Gas	Gas Evolution (cm^3)		Vol_{PL}/Vol_{PCP}
	Porous Liquid (PL)	Hexachloropropene (PCP)	
N_2	2.10 ± 0.20	0.22	9.54
CH_4	6.33 ± 0.21	0.3	21.1
CO_2	7.53 ± 0.47	0.3	25.1
Xe	10.05 ± 0.21	0.45	22.33

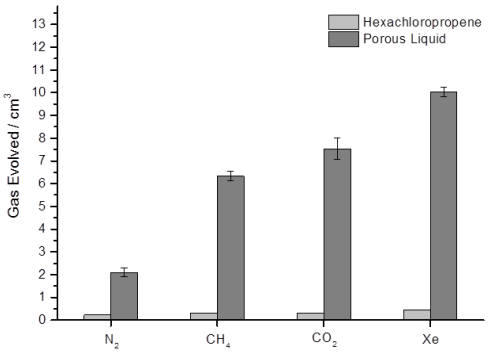

Supplementary Figure 33. Gas evolution measurements for hexachloropropene *vs* the scrambled porous liquid by displacement with 1 molar equivalent of chloroform. For all gases around ten to twenty times as much gas is evolved from the porous liquid compared to the non-porous hexachloropropene solvent.

Gas	Mean gas evolution ± SD (cm^3)	
	Excess $CHCl_3$	1.0 eq. $CHCl_3$
N_2	1.57 ± 0.08	2.10 ± 0.20
CH_4	5.60 ± 0.3	6.33 ± 0.21
CO_2	4.25 ± 0.13	7.53 ± 0.47
Xe	–	10.05 ± 0.21

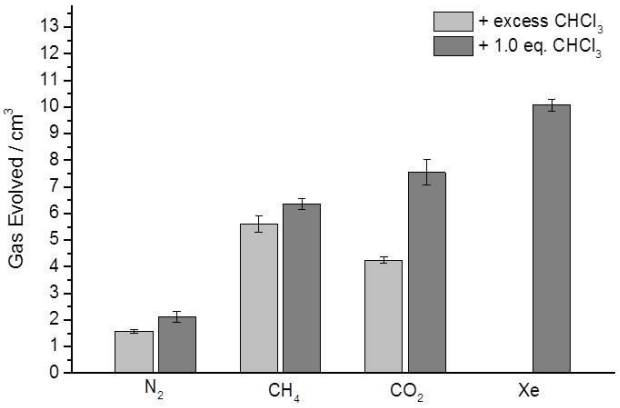

Supplementary Figure 34. Gas evolution measurements for the scrambled porous liquid. Average volumes of gas collected by displacement are reported, using either an excess of chloroform (left column) or one molar equivalent of chloroform based on the scrambled cage (right column). For xenon, only the 1 mole equivalent test was made. In general, 1.0 mole equivalent of $CHCl_3$ is more effective for gas displacement from the cage, presumably because larger, excess volumes of $CHCl_3$ partially dissolve the gas that is being displaced. This is particularly evident in the case of CO_2.

Gas	Average gas evolved (cm^3)	Occupancy based on gas evolution (%)
N_2	2.1	15.2
CH_4	6.33	45.8
CO_2	7.53	54.5
Xe	10.05	72.8

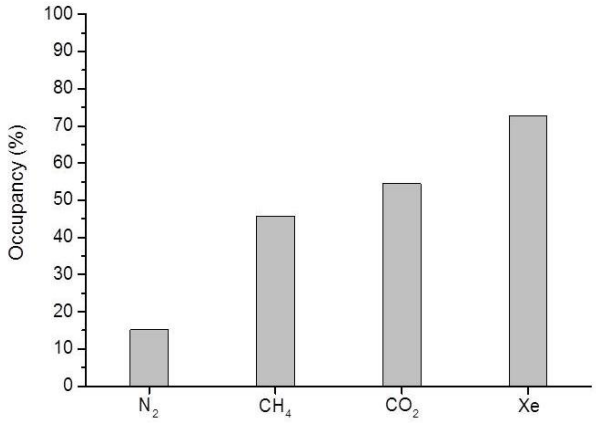

Supplementary Figure 35. Gas occupancies in the scrambled cages porous liquid. From the volumes of gas evolved in the 1 mol. eq. $CHCl_3$ displacement studies (**Supplementary Figure 34**), it is possible to estimate the occupancy of the scrambled cages. This makes the simple assumption that all of the gas molecules reside inside cages, which may not be the case (see *e.g.*, **Supplementary Figure 19**, which shows simulated methane locations for the crown-ether cage porous liquid). If we assume occupancy of 1 gas molecule per host cage, then we can calculate that the theoretical amount of gas evolved will be 13.8 cm^3 (20 % w/v solution; 600 mg of scrambled cage in 3 mL hexachloropropene), assuming that 100% of the gas is displaced by $CHCl_3$ addition (1 mol. eq.). This allows us to calculate an average occupancy for N_2, CH_4, CO_2 and Xe. The average cage occupancy increases from 15.2 % for N_2 to 45.8 % for CH_4. The average occupancy for CO_2 is 54.5 %, and for Xe it is 72.8 %. The gas absorption properties of this porous liquid therefore mirror the properties of analogous porous cage solids. For example, solid **CC3**-*R* has a very high affinity for Xe, which is a near-optimal fit within the cage cavity.[26] The calculated isosteric heats of adsorption for solid **CC3**-*R* for these four gases are as follows:[26]

N_2 = 17.14 kJ/mol; CH_4 = 22.05 kJ/mol; CO_2 = 27.73 kJ/mol; Xe = 31.31 kJ/mol

These isosteric heats comprise both adsorption within the cage cavities, and also adsorption at sites between neighbouring cages. While the latter may be less prevalent for porous liquids, the correlation between average cage occupancy and the isosteric heats for analogous cage solids suggests that the interaction of the gas with the cage cavity dominates gas solubility in these liquids.

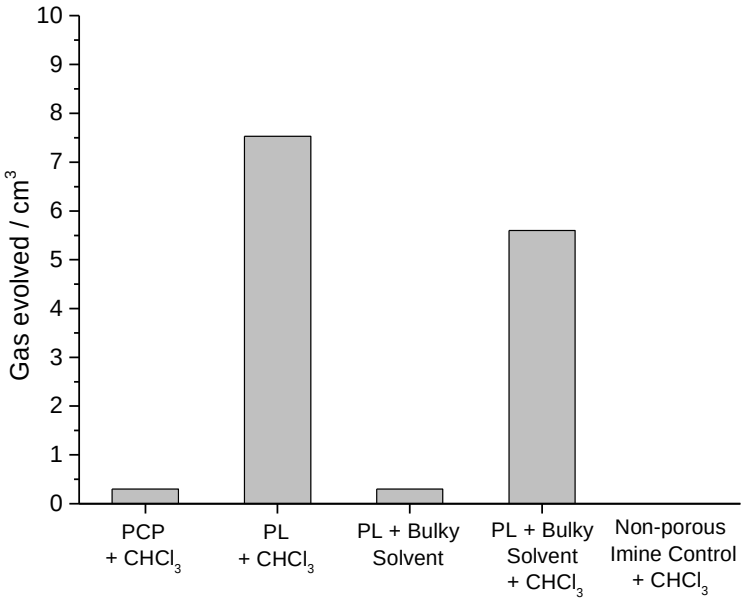

Supplementary Figure 36. Guest selectivity in 'scrambled' porous liquids. CO_2 (green bar; 7.5 cm^3) is evolved by addition of a 1 mol. eq. of $CHCl_3$ to a CO_2-saturated solution of scrambled porous liquid (PL). By contrast, addition of a bulky solvent (1 mol. eq. 1-*t*-butyl-3,5-dimethylbenzene) displaces almost no gas (0.3 cm^3). Subsequent addition of $CHCl_3$ releases CO_2 gas (5.6 cm^3). This illustrates that this porous liquid is guest selective, like porous solids such as zeolites, even though it is an isotropic fluid.

Supplementary Video 1. Guest selectivity in 'scrambled' porous liquids. Two batches of porous liquid were prepared in vials (200 mg cage dissolved in 1 mL hexachloropropene, prepared according to the standard procedure) and both were saturated with xenon gas (5 min bubbling at 50–60 mL/min, regulator output pressure set to 0.5 bar and flow fine-controlled with needle valve to 60–66 on Gilmont flowmeter scale with a stainless steel float), followed by the addition of a stirrer bar. To one sample was carefully added chloroform (16 μL, 1.0 mol. eq. based on cage) and to the other was added 1-*t*-butyl-3,5-dimethylbenzene (36 μL, 1.0 mol. eq.), in both cases being careful not to mix the solvents. Stirring was then started to mix the solvent layers – as can be observed in the video, chloroform displaces the xenon gas whereas the large, bulky solvent does not.

7. Supplementary References & Notes

1. Bogatsky, A. V., Lukyanenko, N. G., Lobach, A. V., Nazarova, N. Yu. & Karpenko, L. P. *Synth. Commun.*, 139 (1984).

2. Jorgensen, W. L., Maxwell, D. S. & Tirado-Rives, J. Development and testing of the OPLS all-atom force field on conformational energetics and properties of organic liquids, *J. Am. Chem. Soc.* **118**, 11225 (1996).

3. Jorgensen, W. L. & Tirado-Rives, J. Potential energy functions for atomic-level simulations of water and organic and biomolecular systems, *Proc. Natl. Acad. Sci. U. S. A.* **102**, 6665 (2005).

4. Frenkel, D. & Smit, B. Understanding molecular simulation, Academic Press, Inc., 2nd edn, 2001.

5. Roux, B. The calculation of the potential of mean force using computer-simulations, *Comput. Phys. Commun.* **91**, 275 (1995).

6. Kumar, S., Rosenberg, J. M., Bouzida, D., Swendsen, R. H. & Kollman, P. A. Multidimensional free-energy calculations using the weighted histogram analysis method, *J. Comput. Chem.* **13**, 1011 (1992).

7. Hess, B., Kutzner, C., van der Spoel, D. & Lindahl, E. GROMACS 4: Algorithms for highly efficient, load-balanced, and scalable molecular simulation, *J. Chem. Theory Comput.*, **4**, 435 (2008).

8. Nose, S. A molecular-dynamics methods for simulations in the canonical ensemble, *Mol. Phys.* **52**, 255 (1984).

9. Hoover, W. G. Canonical dynamics - equilibrium phase-space distributions, *Phys. Rev. A: At., Mol., Opt. Phys.*, **31**, 1695 (1985).

10. Parrinello, M. & Rahman, A. Polymorphic transitions in single-crystals - a new molecular-dynamics method, *J. Appl. Phys.*, **52**, 7182 (1981).

11. Essmann, U., Perera, L., Berkowitz, M. L., Darden, T., Lee, H. & Pedersen, L. G. A smooth particle mesh Ewald method, *J. Chem. Phys.* **103**, 8577 (1995).

12. Pohorille, A. & Pratt, L. R. Cavities in molecular liquids and the theory of hydrophobic solubilities, *J. Am. Chem. Soc.* **112,** 5066 (1990).

13. Pratt, L. R. & Pohorille, A. Theory of hydrophobicity - transient cavities in molecular liquids, *Proc. Natl. Acad. Sci. U. S. A.* **89**, 2995 (1992).

14. Shaikh, M. Q., Rätzke, K. Gaukler, J. Ch., Possart, W. & Faupel, F. Reactive epoxies with functional zeolite fillers: IR spectroscopy and PALS studies, *J. Mater. Res.* **26**, 2877 (2011).

15. Kruse, J., Rätzke, K., Faupel, F., Sterescu, D. M., Stamatialis, D. F. & Wessling, M. Free volume in C_{60} modified PPO polymer membranes by positron annihilation lifetime spectroscopy, *J. Phys. Chem. B*, **111**, 13914 (2007).

16. Harms, S., Rätzke, K., Faupel, F., Schneider, G. J., Willner, L. & Richter, D. Free volume of interphases in model nanocomposites studied by positron annihilation lifetime spectroscopy, *Macromolecules* **43**, 10505 (2010).

17. Kansy, J. Microcomputer program for analysis of positron annihilation lifetime spectra, *Nucl. Instrum. Methods A* **374**, 235 (1996).

18. Mahmood, T., Cheng, K. L. & Yean, Y. C. Microanalysis of open spaces in crown ethers by using a novel probe: Positron annihilation spectroscopy, *Third International Workshop on Positron and Positronium Chemistry*, 640 (1990).

19. Jacquemin, J., Costa Gomes, M. F., Husson, P. & Majer, V. Solubility of carbon dioxide, ethane, methane, oxygen, nitrogen, hydrogen, argon, and carbon monoxide in 1-butyl-3-methylimidazolium tetrafluoroborate between temperatures 283 K and 343 K and at pressures close to atmospheric, *J. Chem. Thermodynamics* **38**, 490 (2006).

20. The volume of liquid solvent was calculated by using the density for 15-crown-5 at 20 °C of 1.113 $g \cdot cm^{-3}$, as reported in the *CRC Handbook of Chemistry and Physics*.

21. The second virial coefficient for methane was taken from Dymond, J. & Smith, E. B. The virial coefficients of pure gases and mixtures, Clarendon Press, Oxford, 1980.

22. M.F. Costa Gomes. Low pressure solubility and thermodynamics of solvation of carbon dioxide, ethane and hydrogen in 1-hexyl-3-ethyl-imidazolium bis[(trifluoromethyl)sulfonyl]amide between temperatures 283 K and 343 K. *J. Chem. Eng. Data* **52**, 472 (2007).

23. Hasell, T., Culshaw, J. L., Chong, S. Y., Schmidtmann, M., Little, M. A., Jelfs, K. E., Pyzer-Knapp, E. O., Shepherd, H., Adams, D. J., Day, G. M., Cooper, A. I. Controlling the crystallization of porous organic cages: Molecular analogs of isoreticular frameworks using shape-specific directing solvents. *J. Am. Chem. Soc.* **136**, 1438 (2014).

24. Tozawa, T., Jones, J. T. A., Swamy, S. I., Jiang, S., Adams, D. J., Shakespeare, S., Clowes, R., Bradshaw, D., Hasell, T., Chong, S. Y., Tang, C., Thompson, S., Parker, J., Trewin, A., Bacsa, J., Slawin, A. M. Z., Steiner, A., Cooper, A.I. Porous organic cages. *Nat. Mater.* **8**, 973 (2009).

25. Jiang, S., Jones, J. T. A., Hasell, T., Blythe, C. E., Adams, D. J., Trewin, A., Cooper, A. I. Porous organic molecular solids by dynamic covalent scrambling. *Nat. Commun.* **2**, 207 (2011).

26. Chen, L., Reiss, P. S., Chong, S. Y., Holden, D., Jelfs, K. E., Hasell, T., Little, M. A., Kewley, A., Briggs, M. E., Stephenson, A., Thomas, K. M., Armstrong, J. A., Bell, J., Busto, J., Noel, R., Liu, J., Strachan, D. M., Thallapally, P. K., Cooper, A. I. Separation of rare gases and chiral molecules by selective binding in porous organic cages. *Nat. Mater.* **13**, 954 (2014).